

LIBRARY Michigan State University

This is to certify that the

thesis entitled

FLOW LINE FORMATION OF INJECTION MOLDED POLYPROPYLENE/EP RUBBER BLENDS

presented by

Paul Andrew Papworth

has been accepted towards fulfillment of the requirements for

M.S. degree in Chemical Engineering

Date 8/31/01

MSU is an Affirmative Action/Equal Opportunity Institution

0-7639

PLACE IN RETURN BOX to remove this checkout from your record.

TO AVOID FINES return on or before date due.

MAY BE RECALLED with earlier due date if requested.

DATE DUE	DATE DUE	DATE DUE
(PR 1 102804		

6/01 c:/CIRC/DateDue.p65-p.15

# FLOW LINE FORMATION OF INJECTION MOLDED POLYPROPYLENE/EP RUBBER BLENDS

Ву

Paul Andrew Papworth

### A THESIS

Submitted to
Michigan State University
In partial fulfillment of requirements
For the degree of

MASTER OF SCIENCE

Department of Chemical Engineering

2001

#### **ABSTRACT**

## FLOW LINE FORMATION OF INJECTION MOLDED POLYPROPYLENE/EP RUBBER BLENDS

#### By

#### Paul Andrew Papworth

Flow line formation (typically referred to as tigerstriping) is a common manufacturing problem of injection molded materials. This study investigates the morphology of two polymer blends containing polypropylene and one of two different grades of ethylene propylene (EP) rubber. Image analysis of SEM micrographs from short shots taken at the flow mark surface, out-of-flow mark surface, and cross-sectional core behind the flow front regions reveals EP rubber particles with various degrees of stretching from the core to the mold wall regions. From a detailed analysis of the micrographs, a mechanism for flow line formation is proposed. As the mold is filled, an asymmetric melt front forms and the melt head strays from the centerline creating a long and short span. If the EP rubber particles flow along the short span, they simultaneously coalesce, become stretched to their maximum, and become frozen at the mold wall to form the out-of-flow mark region. If the particles flow along the long span, there is enough time for them to simultaneously coalesce and stretch to their maximum, and then partially retract. As the partially retracted particles reach the mold wall, they freeze to form a flow mark region. Both materials studied exhibited evidence of particle stretching, coalescing, and retracting in the flow mark regions. A 25% reduction of the interfacial area of the particles from the out-of-flow mark to flow mark regions was observed in both materials.

In Loving Memory of My Father, Charles Richard Papworth II Who Did Not Live Long Enough to See His Son Graduate

#### **ACKNOWLEDGMENTS**

This research was supported by Montell Polyolefins and I am please to acknowledge Dr.

Chi Chang Shu for his assistance in identifying materials and providing the SEM micrographs for study.

I'd also like to thank Dr K. Jayraman for his insight and guidance to me during this project. I've learned more from my conversations with him about engineering than I ever have from a book.

Lastly, I would like to thank my mother, father, and three brothers Skip, Kyle, and Drew for their support and encouragement over the years. I would also like to thank Guangda, Darrel, Sang-Yoon, Jason, and Jon for making grad school fun. I'd especially like to thank my two friends Frank and Kevin for helping me blow off some steam when I needed too.

## **TABLE OF CONTENTS**

LIST OF TABLES		<b>v</b> i
LIST OF FIGURES	S	vii
LIST OF SYMBOL	.S	ix
CHAPTER 1		
	ness Work	
_	d Mechanism Statement	
CHAPTER 2		
	OF POLYPROPYLENE/EP RUBBER BLENDS	
	l Properties	
	nalysis	
	of TPO #1 Image Analysis	
	TPO #1 Particle Shapes	
	Flow Mark vs. Out-of-flow Mark Comparison	
	Core Flow Front vs. Mold Wall Comparison	
	of TPO #2 Image Analysis	
	TPO #2 Particle Shapes	
	Flow Mark vs. Out-of-flow Mark Comparison	
	Core Flow Front vs. Mold Wall Comparison	
CHAPTER 3		
	ND RECOMMENDATIONS	
	sions	
3.2 Recomm	nendations for Further Work	65
APPENDICES		
	E ANALYSIS	
	ation of Aspect Ratio	
2. Determin	ation of x, y, and z Dimensions	69
RIRI IOCRAPHY		71

## LIST OF TABLES

Table 2.1 Material properties of TPO #1 and #2 blends	7
Table 2.2 Out-of-flow mark region comparison of particles less than 5 μm <sup>2</sup> vs. greater than 5 μm <sup>2</sup> .	17
<b>Table 2.3</b> Flow mark region comparison of particles less than $5 \mu m^2$ vs. greater than $5 \mu m^2$	21
Table 2.4 Measured values and calculated statistics for particles in TPO #1	28
Table 2.5 Geometric equations for various particle shapes	29
Table 2.6 Variability of x, y, and z dimension lengths for TPO #1	31
Table 2.7 Number average for the out-of-flow mark and flow mark regions	32
Table 2.8 Average particle dimensions for the core flow front region	37
Table 2.9 TPO #2 Out-of-flow mark region comparison of particles less than 7 μm <sup>2</sup> vs. greater than 7 μm <sup>2</sup>	40
<b>Table 2.10</b> TPO #2 Flow mark region comparison of particles less than $7 \mu m^2$ vs. greater than $7 \mu m^2$ .	44
Table 2.11 Measured values and calculated statistics for particles in TPO #2	51
Table 2.12 Variability of x, y, and z dimension lengths for TPO #2	54
Table 2.13 Number averaged statistics for the out-of-flow mark and flow mark regions	55
Table 2.14 Average particle dimensions for the core flow front region	60
Table 3.1 Effects of changing the molding conditions on flow line formation	65

## **LIST OF FIGURES**

Figure 1.1	Flow	lines on the face and reverse sides of a rectangular mold	2
_		sectional melt front deformation showing the formation of the long	
Figure 2.1	Tensil	e bar dimensions	o
rigure 2.1	1 611511	e dar dimensions	o
Figure 2.2	Flow l	ine patterns for (a) TPO #1 and (b) TPO #2	8
Figure 2.3	Micro	graph locations	9
	1. Out	-of-flow mark on the plaque surface (in the xy plane)	9
		w mark on the plaque surface (in the xy plane)	
		ss-section at the wall underneath the flow mark (in the xz plane)	
	4. Cro	ss-section at the wall underneath the out-of-flow mark (in the xz	
		ne)	
	5. Cro	ss-section behind the flow front (in the xz plane)	9
Figure 2.4	Out-of	-flow mark surface morphology for TPO #1	10
	(a)	0.44" short shot	10
	(b)	0.52" short shot	10
	(c)	0.58" short	10
Figure 2.5	Flow r	mark surface morphology for TPO #1	11
	(a)	0.44" short shot	11
	(b)	0.52" short shot	11
	(c)	0.58" short	11
Figure 2.6	Cross	sectional core flow front morphology for TPO #1	12
	(a)	0.44" short shot	
	(b)	0.52" short shot	12
	(c)	0.58" short	12
Figure 2.7	Out-of	-flow mark surface morphology for TPO #2	13
_		0.50" short shot	
	(b)	0.53" short shot	13
Figure 2.8	Flow r	nark surface morphology for TPO #2	13
80	(a)	0.50" short shot	
	` '	0.53" short shot	
Figure 2.9	Cross	sectional core flow front morphology for TPO #1	14
-	(a)	0.50" short shot	

	(b) 0.53" short shot	4
Figure 2.10	(a) Out-of-flow mark surface micrograph	l6 l6
Figure 2.11	Aspect ratio distributions for the out-of-flow mark region of TPO #1 1	8
	TPO #1 out-of-flow mark region particle lengths in the x and y directions om Figure 2.2(a))	18
Figure 2.13	Cross-sectional morphology at the mold wall in the x, z plane for TPO #1	9
Figure 2.14	Aspect ratio distributions for the flow mark region of TPO #12	22
	TPO #1 flow mark region particle lengths in the x, y, and z dimensions om Figures 2.2(c) and 2.5(b))	22
Figure 2.16	Particle orientation distribution for the flow mark region of TPO #1 2	23
Figure 2.17	(a) Cross-sectional morphology at the core flow front for TPO #1	
Figure 2.18	Aspect ratio distribution for the core flow front region of TPO #12	!4
	TPO #1 core flow front region particle lengths in the x and z dimensions om Figure 2.8)	25
Figure 2.20	Circular cylinder particle in the out-of-flow mark region	<u>!</u> 6
Figure 2.21	Elliptical cylinder particle in the flow mark region	:6
Figure 2.22	Ellipsoid particle in the core flow region	!7
Figure 2.23	Particle size area distribution for TPO #1	!9
Figure 2.24	Particle size distribution for TPO #1	0
Figure 2.25	Aspect ratio distributions for TPO #13	0
Figure 2.26	(a) Out-of-flow mark surface micrograph	1

	(d) Detail of individual particles in the flow mark surface region	41
Figure 2.27	Aspect ratio distributions for the out-of-flow mark region of TPO #2	42
•	TPO #2 Out-of-flow mark region particle lengths in the x, y, and (measured from Figures 2.17(a) and 2.20(a))	42
	Cross-sectional morphology at the mold wall in the x, z plane for	43
Figure 2.30	Aspect ratio distributions for the flow mark region of TPO #2	. 45
	TPO #2 flow mark region particle lengths in the x, y, and z directions rom Figures 2.17(c) and 2.20(b))	45
Figure 2.32	Flow mark particle orientation distribution for TPO #2	. 46
Figure 2.33	(a) Cross-sectional morphology at the core flow front for TPO #2	
Figure 2.34	Aspect ratio distribution for the core flow front region of TPO #2	. 47
•	TPO #2 core flow front region particle lengths in the x and z directions rom Figure 2.33)	. 48
Figure 2.36	Elliptical cylinder particle in the out-of-flow mark region	. 49
Figure 2.37	Elliptical cylinder particle in the flow mark region	. 49
Figure 2.38	Ellipsoid particle in the core flow region	. 49
Figure 2.39	Particle size area distributions for TPO #2	. 52
Figure 2.40	Particle size distributions for TPO #2	. 52
Figure 2.41	Aspect ratio distributions for TPO #2	. 53

#### LIST OF SYMBOLS

a Minor axis  $A_I$  Interfacial area

A<sub>I TOTAL</sub> Total interfacial area

 $A_i$  Particle area

 $A_{xy}$  Projected area in the xy plane  $A_{xz}$  Projected area in the xz plane  $A_{yz}$  Projected area in the yz plane

b Major axis

 $\overline{b}$  Average length of b c y direction length

D Diameter

EP Ethylene propylene  $L_x$  x direction length  $L_z$  z direction length MW Molecular weight

 $N_C$  Total number of particles in the Core Flow Front Region

 $N_{FM}$  Total number of particles in the Flow Mark Region

N<sub>OOFM</sub> Total number of particles in the Out-Of-Flow Mark Region

 $\pi$  Pi

PP Polypropylene

R Radius

RIM Reaction injection molded
SEM Scanning electron microscope
TEM Transmission electron microscope

TPO Thermoplastic olepfins

 $V_T$  Total particle volume

x Flow direction

 $x_{AWA}$  x direction area weighted average length

 $x_{NA}$  x direction number averaged length

y Tranverse flow direction

 $y_{AWA}$  x direction area weighted average length

 $y_{NA}$  y direction number averaged length

z Gap direction

 $z_{AWA}$  x direction area weighted average length

 $z_{NA}$  z direction number averaged length

#### CHAPTER 1

#### INTRODUCTION

With the increasing use of exotic plastics, polymer blends, and polymer composites in the automotive manufacturing process, a common problem is the formation of surface defects on injection-molded parts. Polymers used to make bumpers, specific body parts, and interior components need a class A finish (within plain sight of the driver) and therefore they must be free of any aesthetic defects. Such defects on injection-molded polymer parts can take many different forms but this study will focus on flow lines (alternating bands of gloss and dullness along the parts surface, commonly referred to as "tigerstriping") in thermoplastic olefins (TPO's). Flow lines (transverse to the main flow) are frequently formed on the surface of injection-molded thermoplastics. This effect can be observed using neat polypropylene, if the injection molding conditions are pushed far enough, but the problem is much more common when the injected material is a polymer blend, a TPO, or a filled polymer (Han et al., 1996; Hobbs, 1996). The material studied is a blend of polypropylene and ethylene propylene (EP) rubber that combines the stiffness and structural characteristics of the polypropylene with the flexibility and toughness of EP rubber. These TPO blends are replacing reaction injection molded (RIM) polyurethanes because they provide better impact strength and paint durability properties on the final molded parts.

### 1.1 Flow Lines

Flow lines are a common problem in the manufacturing of injection molded thermoplastics. The surface has repeating alternating bands of gloss; the good area has a high gloss finish while the flow lines have lower gloss and a dull appearance (Hamada, 1996). Comparing the face side and the back side of a rectangular molded part, the band pattern is phase shifted 180 degrees, i.e., when one side has a high gloss area, the opposite side has low gloss, even with symmetric mold cavities (Figure 1.1).

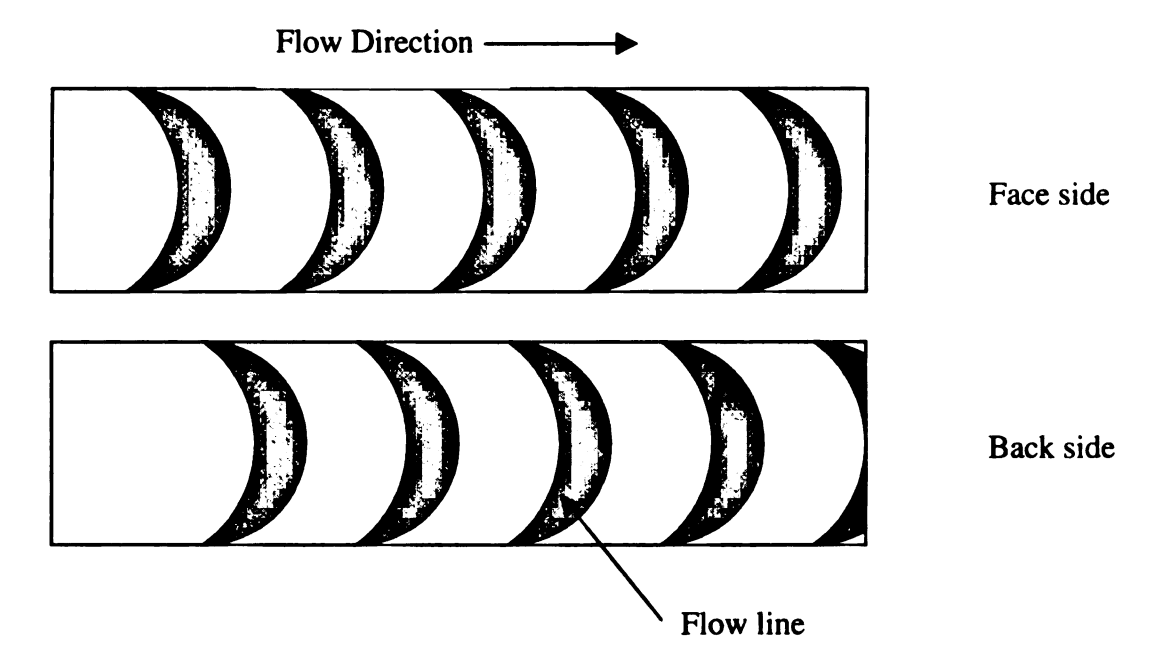


Figure 1.1 Flow lines on the face and reverse sides of a rectangular mold.

### 1.2 Previous Work

The TPO's examined were a two-phase immiscible blend of polypropylene and ethylene propylene (EP) rubber. The EP rubber forms a disperse phase of deformable particles suspended in the polypropylene matrix. The morphological properties of these blends have been studied in order to predict a mechanism for flow line formation. It is believed

that as the mold is filled, the flow becomes unstable from the typical fountain flow pattern, (Himont; 1990) and this unstable flow pattern leads to the formation of flow lines (Chang, 1994; Hamada and Tsunasawa, 1996; Hobbs 1996). Flow near the advancing front is affected by the presence of particles or drops which may deform the melt/air interface significantly under some conditions, leading to surface bumps (Hoffman, 1985; Stoos and Leal, 1989). These bumps, in turn, give rise to asymmetric instabilities in the melt front, which leads to flow line formation. Himont (1990) observed and recorded the melt front deformations using a high-speed camera.

For emulsions containing non-rigid, deformable particles or drops, the morphology can be complicated further by the phenomena of drop break-up, coalescence, and stretching. Bousmina and Muller (1998) studied the rheology and morphology of polymethylmethacrylate rubber blends and found that the degree of stretch of the rubber drops varied going from the center to the wall region. Flow plane micrographs of the extrudate at various positions from the center of the circular conduit were obtained using a transmission electron microscope (TEM). The particles were found to become more stretched and aligned in the direction of the flow when going from the center to the wall. The alignment in the skin region of the extrudate was found to result in a decrease in both viscosity and post-extrusion swell of the blends. Bousmina and Muller did not, however, report any radial concentration variations (i.e., no particle migration).

## 1.3 Proposed Mechanism

As the mold is filled, the melt front starts to deform and the stagnation point begins to oscillate between the two mold walls (Yokoi 1994). The effect of this phenomenon on flow lines is much more noticeable with filled polymers (Hobbs 1996) and polymer blends (Hamada 1996; Han 1996). There are many possible reasons why the melt front deforms in this manner, but that is not the subject of this research. The focus of this study is the resulting morphology differences with polymer blends. The stagnation point drifts away from the centerline as the melt front deforms and approaches one of the mold walls (the top wall will be considered for illustrative purposes). During the oscillation, a long span and short span are created that the EP rubber particles can follow (Figure 1.2).

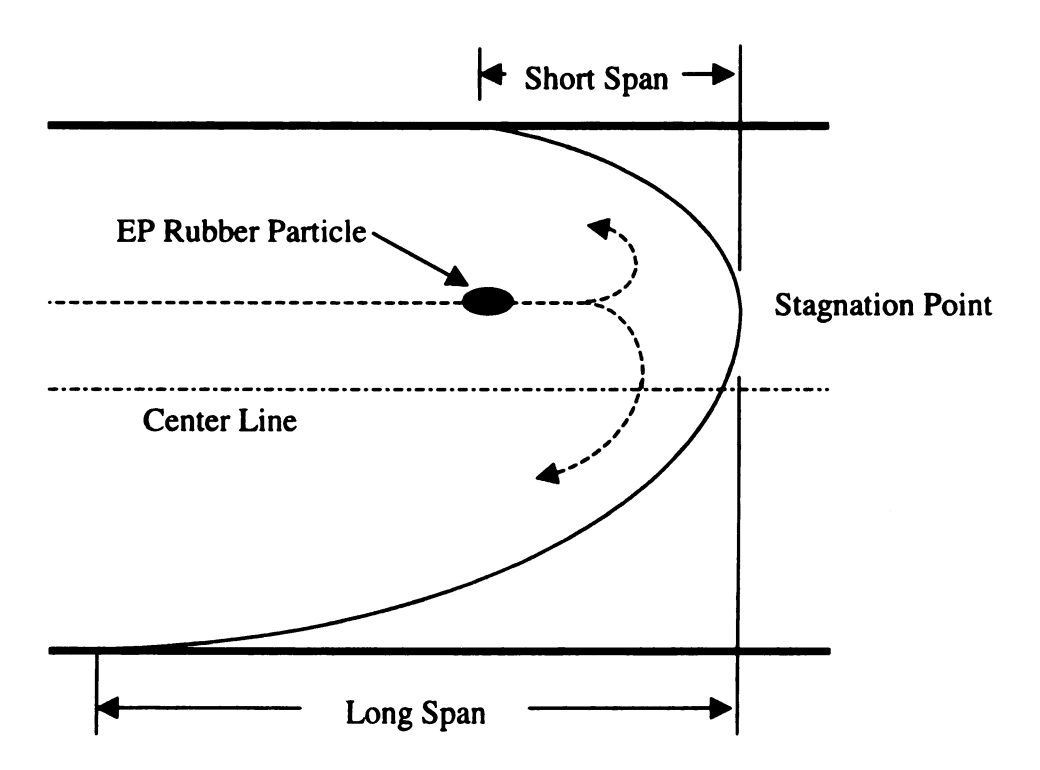


Figure 1.2 Cross-sectional melt front deformation showing the formation of the long and short span.

There are two different cases that can be considered as the particles flow from the melt front to the wall. The first case is that the flow mark region is formed after the particles flow along the short span and an out-of-flow mark region is formed after they flow along the long span. As the EP rubber particles flow along the short span, they undergo biaxial elongational flow. The ellipsoidal core particles are stretched in the x and y directions to form partially stretched drop structures. These incompletely stretched particles then freeze at the mold wall in a random orientation to form a flow mark region. As the particles flow along the long span, they have enough time to fully stretch and align themselves parallel to the flow direction. These highly stretched and oriented particles then freeze at the mold wall to form an out-of-flow mark region.

The second case is that the out-of-flow mark region is formed after the particles flow along the short span and the flow mark region is formed after the particles flow along the long span. If an EP rubber particle follows the short span path, it will stretch to its maximum, align itself parallel the to the flow field, and an out-of-flow mark region will form as the particles freeze at the mold wall. If the particles flow along the long span, the timescale that it takes to flow from the stagnation point to the mold wall is much greater than the timescale for particles flowing along the short span. With this increased timescale, three possible scenarios can occur that form flow lines. Regardless of which scenario occurs, the flow mark particles will be highly oriented in the flow direction. The scenarios are:

• The particles become overstretched, start to break up and tailing occurs. As they reach the bottom wall, the small broken particles freeze to form a flow line.

- The particles are stretched to their maximum, begin to relax, partially retract back,
   and form partially retracted drop structures that are frozen at the mold walls to
   form flow lines.
- The particles are stretched to their maximum, relax, fully retract back, and form fully retracted drop structures that are frozen at the mold walls to form flow lines.

### 1.4 Problem Statement

The focus of this research is to take a detailed look at the dispersed phase morphology of the EP rubber filler of two TPO blends and from the particle sizes, arrive at a conclusion on the dominant mechanism for changes in the particle morphology from the core to the different regions of the surface.

### **CHAPTER 2**

### MORPHOLOGY OF POLYPROPYLENE/EP RUBBER BLENDS

### 2.1 Material Properties

Both TPO blends were compounded in a reactor. Therefore, not all of the individual component material properties are known. Table 2.1 does list the weight percentage of EP rubber in each blend along with the molecular weights of the PP and EP rubber. The solid density is of the PP is 0.908 g/cc. The solid density is of the EP is 0.86 g/cc. Each blend was injection molded into a standard tensile bar mold, the dimensions of which are shown in Figure 2.1. The mold wall temperature was 75°F, the melt temperature was 395°F, and the fill time was eight seconds. Short shots were molded for each material; three for TPO #1 at 0.44, 0.52, and 0.58 inches, and two for TPO #2 at 0.50 and 0.53 inches.

Table 2.1 Material properties of TPO #1 and #2 blends.

TPO	Wt % EP	Volume Fraction	PP MW	EP MW
1	32	0.31	150,000	260,000
2	35	0.34	180,000	235,000

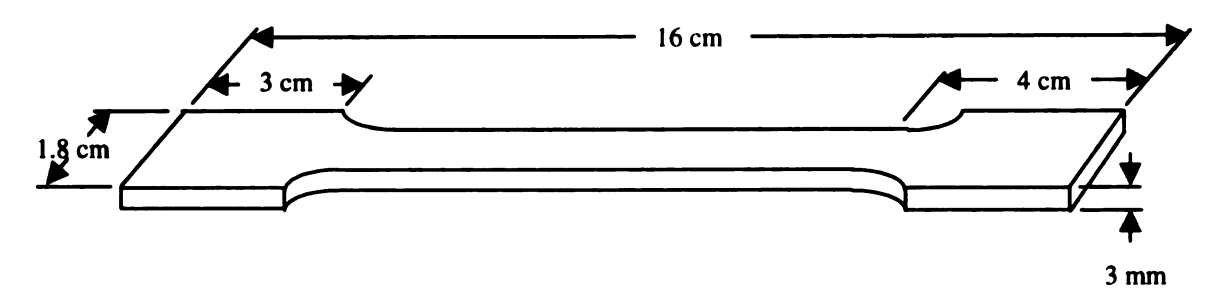


Figure 2.1 Tensile bar dimensions.

The flow line patterns for TPO #1 and #2 are shown in Figure 2.2. For illustrative purposes, the flow mark regions have been colored gray. For TPO #1, the flow line frequency (distance between the centers of two flow lines) is 1.5 cm and the flow line width is 6 mm. For TPO #2, the flow line frequency is 2.0 cm and the flow line width is 11 mm.

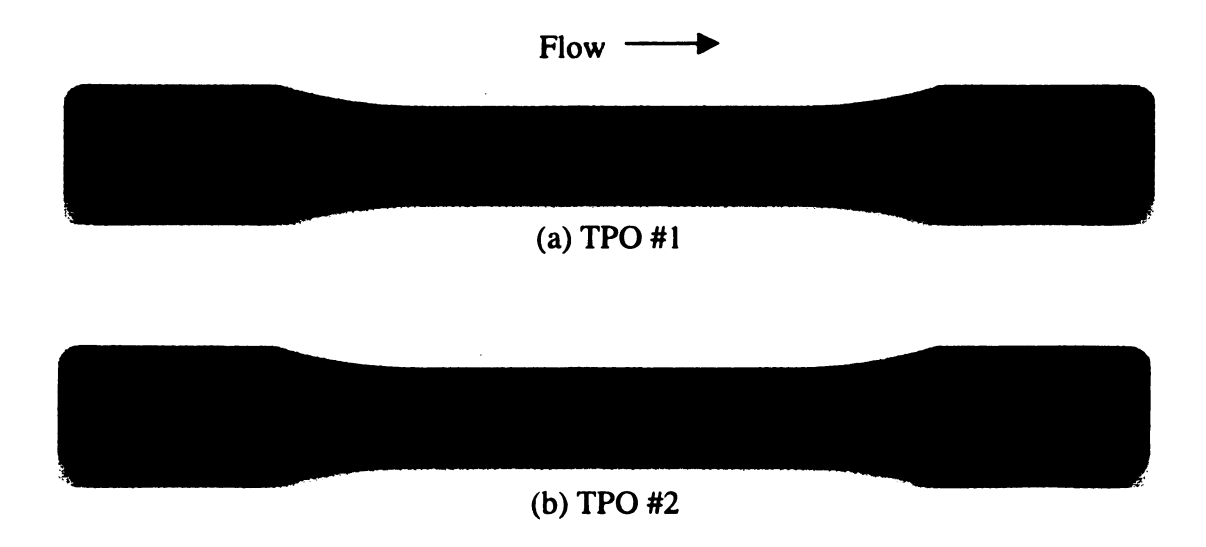


Figure 2.2 Flow line patterns for (a) TPO #1 and (b) TPO #2. (The flow mark regions are shown in gray.)

#### 2.2 SEM Analysis

Montell (Elton, Maryland) provided SEM micrographs for each short-shot. The shortshots were cross-sectioned, microtomed, and the EP rubber was dissolved with methylcyclohexane. The EP rubber particles left dark visible voids in the polypropylene matrix. The micrographs were taken at the locations shown in Figure 2.3 for both TPO's:

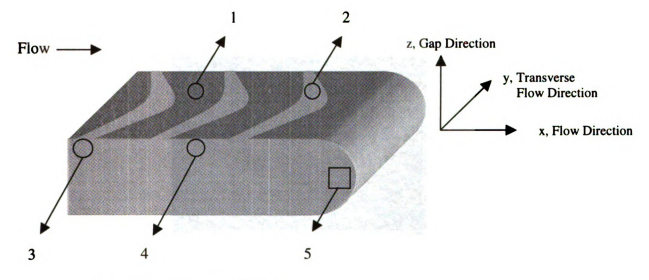


Figure 2.3 Micrograph locations.

- 1. Out-of-flow mark on the plaque surface (in the xy plane)
- 2. Flow mark on the plaque surface (in the xy plane)
- Cross-section at the wall underneath the flow mark (in the xz plane)
- Cross-section at the wall underneath the out-of-flow mark (in the xz plane)
- 5. Cross-section behind the flow front (in the xz plane)

The out-of-flow mark, flow mark, and core flow front region micrographs for each short shot of both TPO's are shown in Figures 2.4-2.9.

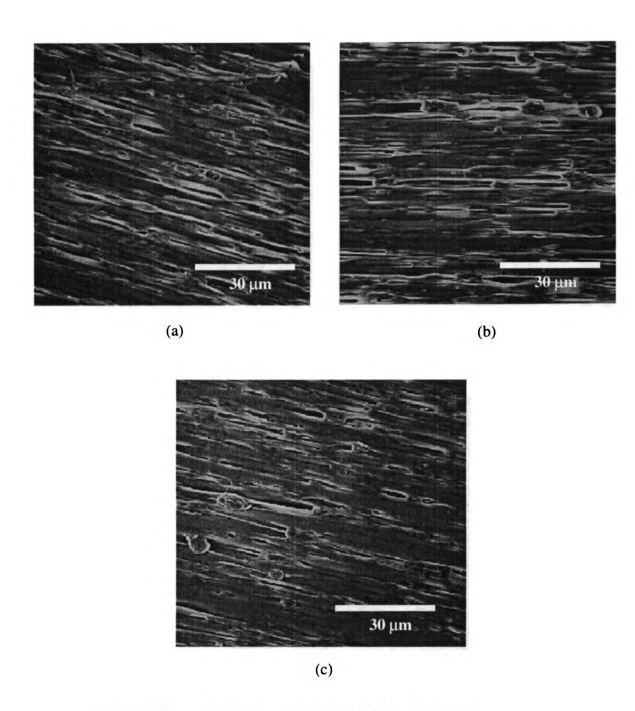


Figure 2.4 Out-of-flow mark surface morphology for TPO #1

(a) 0.44" short shot

- (b) 0.52" short shot
- (c) 0.58" short shot

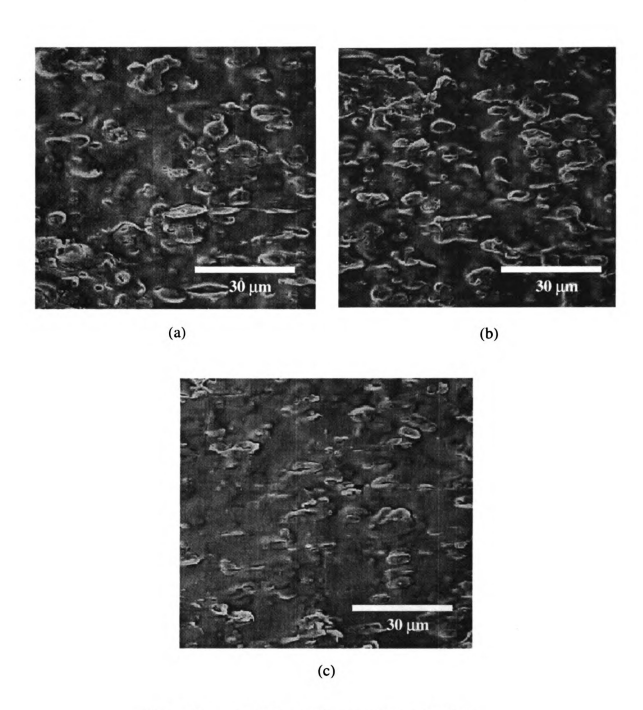
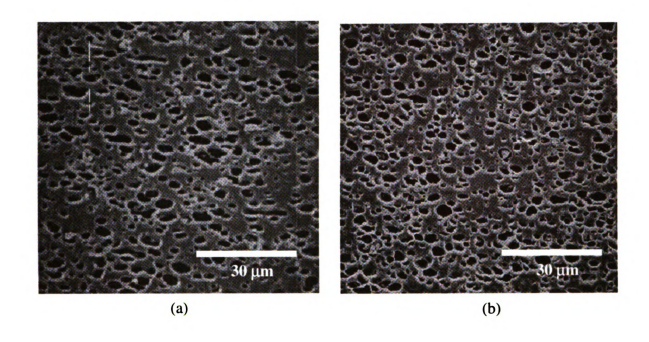


Figure 2.5 Flow mark surface morphology for TPO #1
(a) 0.44" short shot

- (d) 0.52" short shot
- (e) 0.58" short shot



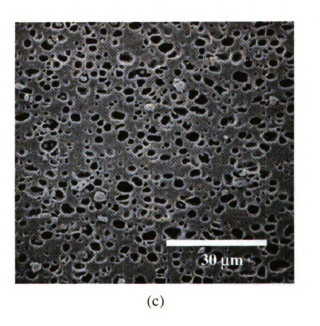


Figure 2.6 Cross sectional core flow front morphology for TPO #1

- (a) 0.44" short shot (b) 0.52" short shot
- (c) 0.58" short shot

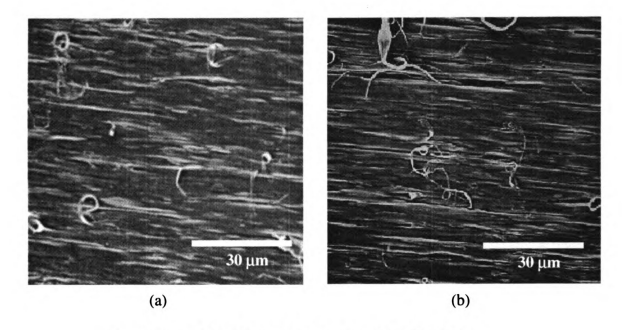


Figure 2.7 Out-of-flow mark surface morphology for TPO #2.

(a) 0.50" short shot

(b) 0.53" short shot

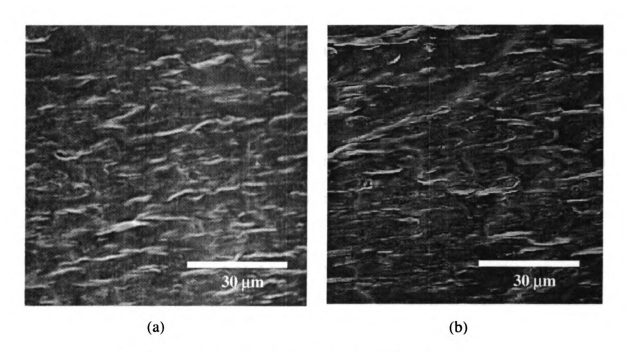


Figure 2.8 Flow mark surface morphology for TPO #2.

(a) 0.50" short shot

(b) 0.53" short shot

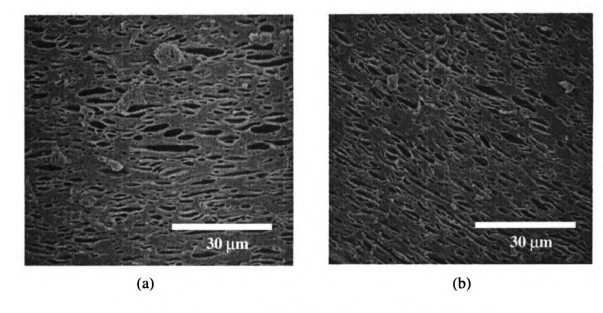


Figure 2.9 Cross sectional core flow front morphology for TPO #2.

(a) 0.50" short shot

(b) 0.53" short shot

All of the micrographs were examined to ensure that the morphology particle shapes observed were consistent in each short shot. Many measurements were made for all the micrographs for each short, but a full set of clear, crisp micrographs showing the x, y, and z dimensions were only obtained for the 0.52 inch short-shot of TPO #1 and the 0.53 inch short-shot of TPO #2. Thus, only these two sets were examined in great detail. The micrographs for TPO #1 are shown in Figures 2.10, 2.13, and 2.17. The micrographs for TPO #2 are shown in Figures 2.26, 2.29, and 2.33. The projected area and the dimensions along the two orthogonal axes were measured for each rubber particle using Jandel Scientifics' Sigma Scan Pro 3.0 and Scion Corporation's Scion Image version 3b image analysis software packages. The out-of-flow mark and flow mark surface pictures were used to determine the particles dimensions in the x and y directions (Figures 2.10

and 2.26). The cross-sectional wall micrographs in the xz plane yielded an average particle thickness in the z direction (Figures 2.13 and 2.29). From these measurements and observations, a three dimensional shape of what the particles at the mold wall might look like was determined.

## 2.3 Results of TPO #1 Image Analysis

Figures 2.10, 2.13, and 2.17 show the micrographs for the out-of-flow mark, flow mark, and core flow front regions. Examination of the particle size distributions, Figures 2.23-2.25, indicates a distinct break at  $5 \, \mu m^2$  in all regions between the presence of small and large particles. Hereafter, small particles will be catorgized by having projected areas  $< 5 \, \mu m^2$  and large particles will have projected areas  $> 5 \, \mu m^2$ .

For the out-of-flow mark surface region (Figure 2.10(a)), the micrographs reveal that the particles are long, narrow, stretched parallel to the flow direction, and have an area fraction of 0.168 (Table 2.2). The large (> 5  $\mu$ m<sup>2</sup>) particles have a high area weighted average aspect ratio of 17.4 and take up 54% of the area fraction in the picture. Examination of the detail, Figure 2.10(b), reveals the presence of many smaller, highly stretched particles. These particles have a much smaller projected area (<< 5  $\mu$ m<sup>2</sup>) but the area weighted average aspect ratio is still large at 12.6. The aspect ratio distribution for all the particles (Figure 2.11) is very wide, ranging from 1-33, with an area weighted average at 15.20.

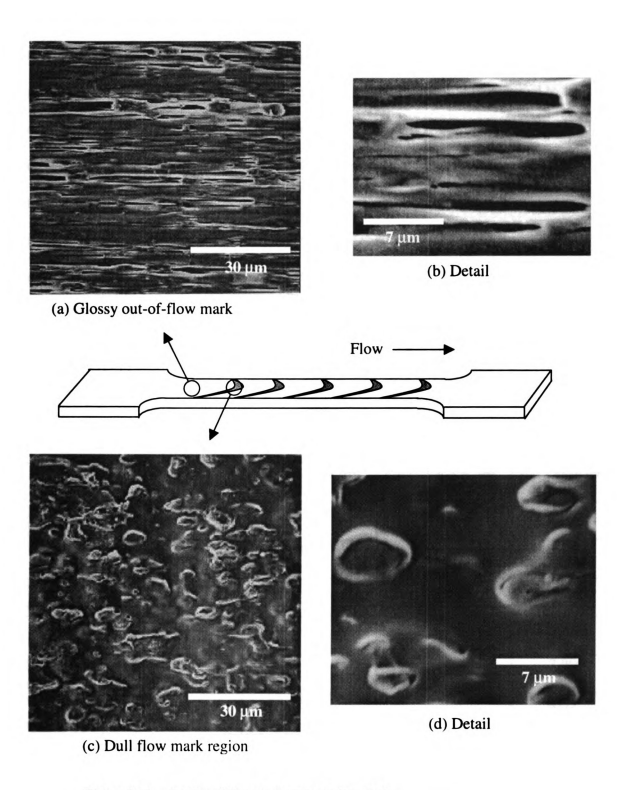


Figure 2.10 (a) Out-of-flow mark surface micrograph.
(b) Detail of individual particles in the out-of-flow mark surface region.

- (c) Flow mark surface micrograph.
- (d) Detail of individual particles in the flow mark surface region.

Table 2.2 compares the small and large particles. It also contains the x and y dimensions that were measured from the paricles in Figure 2.10(a). A value for the z dimension was not obtained from Figure 2.13(a) because not enough particles could be counted to determine a representative thickness for the region. Figure 2.12 shows the x and y dimension distributions for all of the out-of-flow mark particles. Typically, a distribution this wide would indicate that the particle orientation was randomly distributed and that the particles Counted are elliptical slices of particles at random angles. But examination of Figure 10(a) shows that the particles are highly aligned in the flow direction. Even the small particles shown in Figure 10(b) are aligned parallel to flow. Therefore, the aspect ratio distribution is a true measurement of particle length and not an indication of orientation.

**Table 2.2** Out-of-flow mark region comparison of particles less than 5  $\mu$ m<sup>2</sup> vs. greater than 5  $\mu$ m<sup>2</sup>.

	Particles < 5 μm <sup>2</sup>	Particles > 5 μm <sup>2</sup>	All Particles
Projected Area Fraction of Particles	0.077	0.091	0.168
Number of Particles	419	74	493
Number Averaged Aspect Ratio	10.34	18.23	11.53
Area Weighted Aspect Ratio	12.61	17.37	15.20
Number Averaged Areas (μm²)	1.50	10.13	2.80
Weighted Average Areas (μm²)	2.56	12.66	8.05
x-Dimension Area Weighted Averaged Length (µm)	6.01	15.25	11.03
y-Dimension Area Weighted Averaged Length (µm)	0.55	1.11	0.85

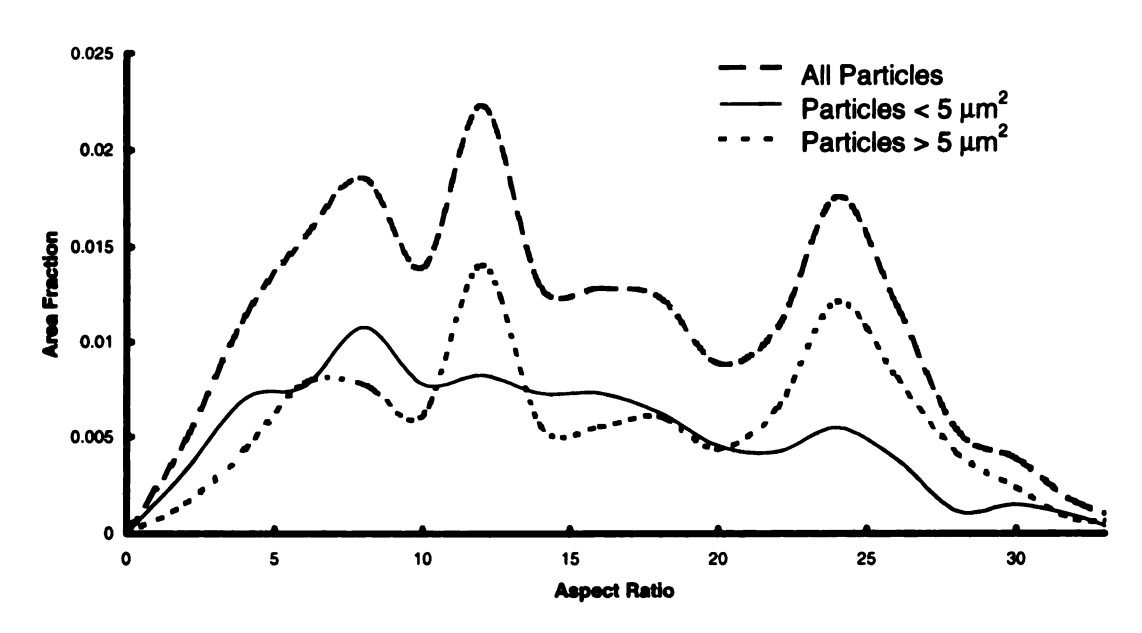


Figure 2.11 Aspect ratio distributions for the out-of-flow mark region of TPO

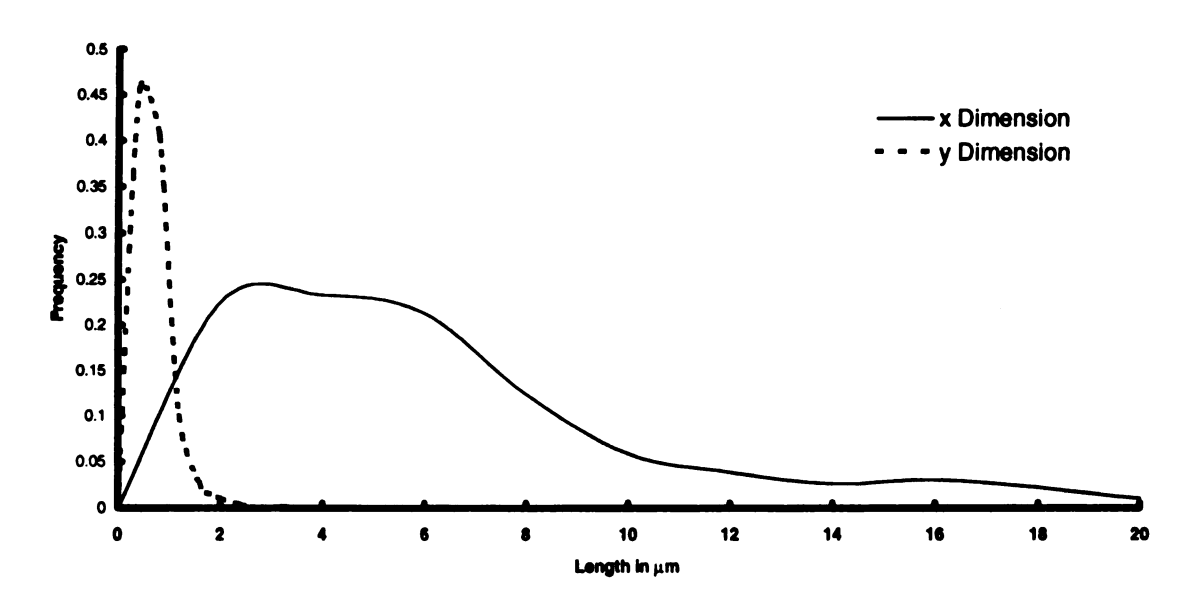


Figure 2.12 TPO #1 out-of-flow mark region particle lengths in the x and y directions (measured from Figure 2.10(a)).

For both the flow mark and out-of-flow mark xz plane pictures at the mold wall (Figure 2.5), only the particles at the mold wall surface were examined to determine an average particle thickness in the z direction for each region. The particles in the xz plane cross section underneath the surface were not counted. All of the particles both regions are aligned parallel to the flow direction. The out-of-flow mark region particles are highly stretched and the flow mark region particles are more globular.

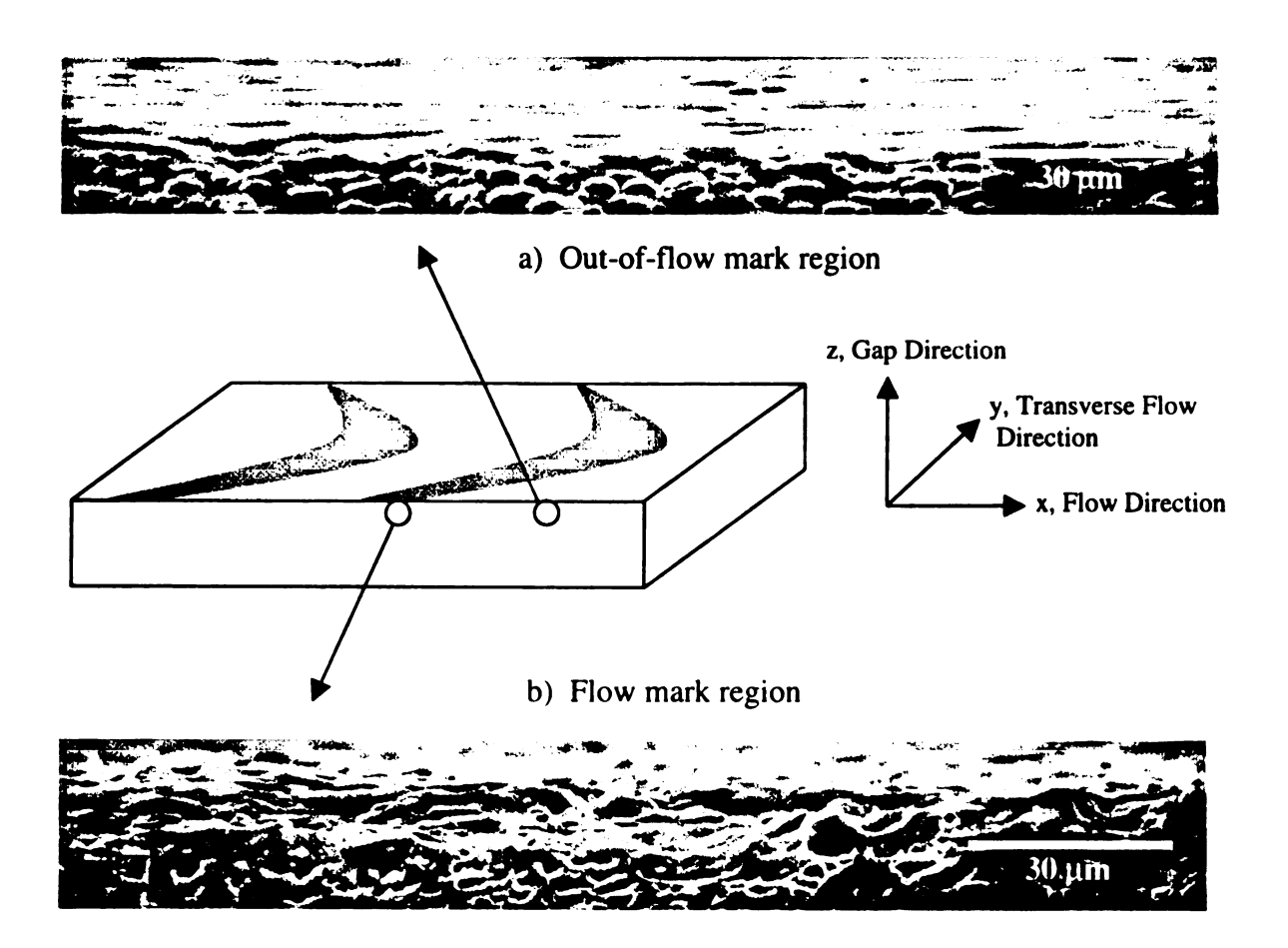


Figure 2.13 Cross-sectional morphology at the mold wall in the x, z plane for TPO

The particles in the flow mark region are elliptical in shape, aligned parallel to the flow direction, and have an area fraction of 0.115 (Table 2.3). The large (>  $5 \mu m^2$ ) particles have a small area weighted aspect ratio of 2.01. The small (<  $5 \mu m^2$ ) particles also have a

small area weighted aspect ratio of 2.13. The aspect ratio distribution (Figure 2.14) for all of the particles is narrow, ranging from 1-5, with an overall area weighted aspect ratio of 2.04. Figure 2.8 shows the particle orientation distribution for all of the flow mark particles. Ther orientations were determined by measuring the angle difference between the paricle's major axis to the flow direction. The Hermann's planar orientation parameter ( $f_p$ ) for TPO #1 is 0.807. It was calculated using:

$$f_p = 2\langle \cos^2 \theta \rangle - 1$$

The small and large particles for the flow mark region are compared in Table 2.3. It also contains the x and y dimensions that were measured from the particles in Figure 2.10(c). The z dimension number averaged length was determined by measuring the thickness of the particles at the mold wall (Figure 2.13). This average thickness was taken as the z dimension of all of the particles, regardless of size. Figure 2.15 shows the x, y, and z dimension distributions for all of the flow mark particles.

Table 2.3 Flow mark region comparison of particles less than 5  $\mu m^2$  vs. greater than 5  $\mu m^2$ .

	Particles < 5 μm <sup>2</sup>	Particles > 5 μm <sup>2</sup>	All Particles
Projected Area Fraction of Particles	0.028	0.087	0.115
Number of Particles	166	64	228
Number Averaged Aspect Ratio	2.18	2.04	2.14
Area Weighted Aspect Ratio	2.13	2.01	2.04
Number Averaged Areas (µm²)	1.41	11.59	4.18
Weighted Average Areas (µm²)	2.66	16.65	13.20
x-Dimension Area Weighted Averaged Length (µm)	2.70	6.69	5.71
y-Dimension Number Averaged Length (μm)	0.92	2.99	1.48
z-Dimension Number Averaged Length (µm)	0.77	0.77	0.77

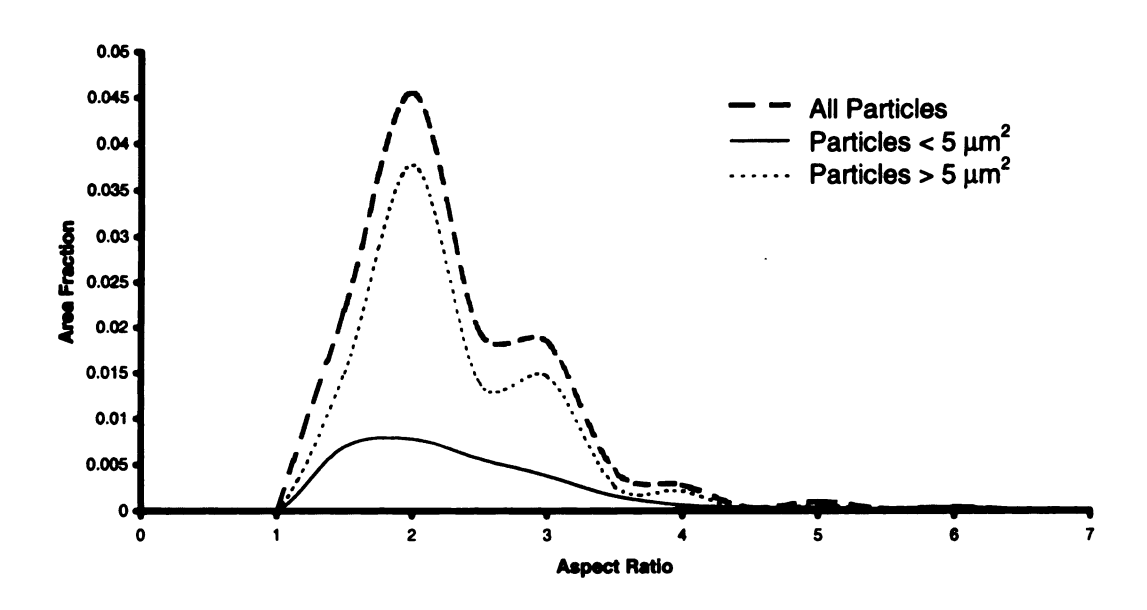


Figure 2.14 Aspect ratio distributions for the flow mark region of TPO #1.

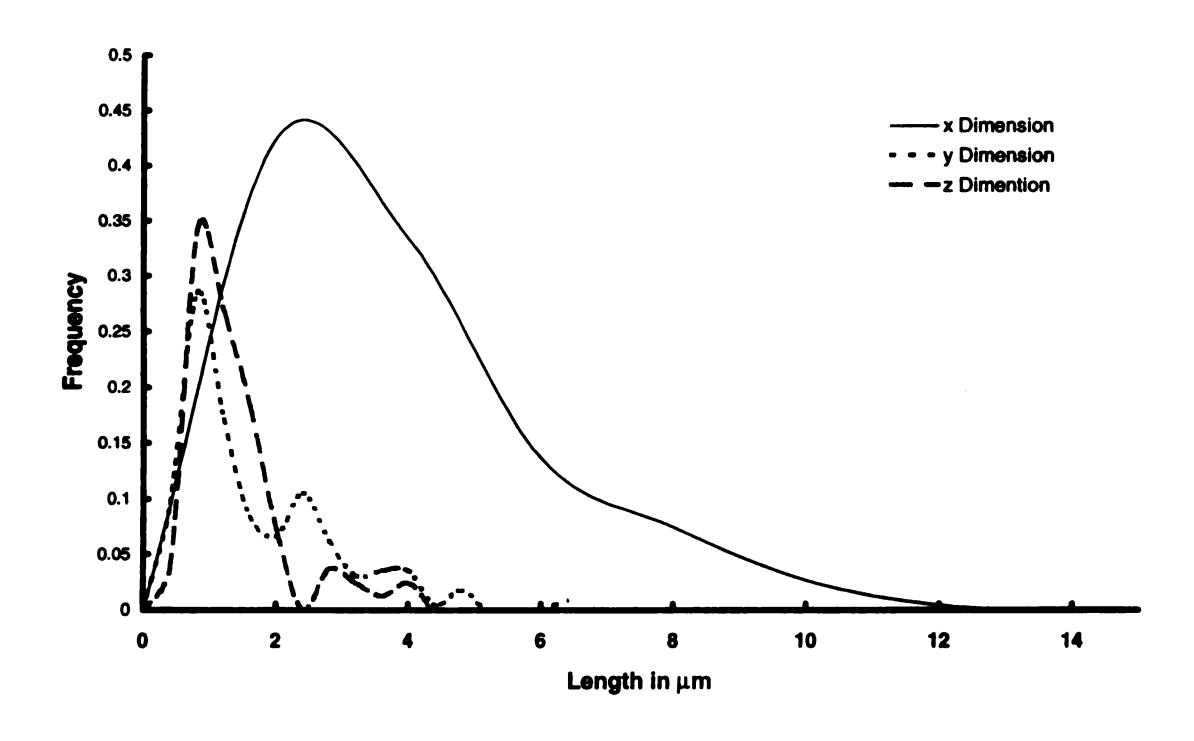


Figure 2.15 TPO #1 flow mark region particle lengths in the x, y, and z dimensions (measured from Figures 2.10(c) and 2.13(b)).

Fo ali

par

(< 5

narro dime

not b

transv

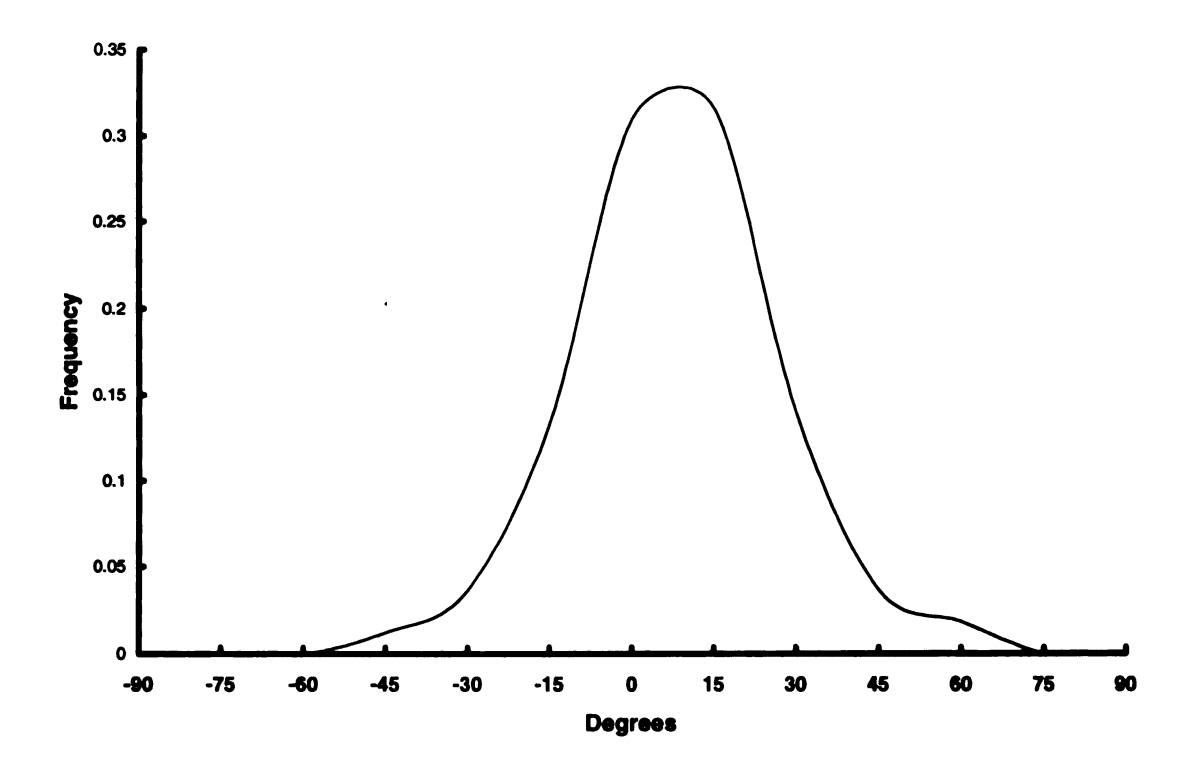


Figure 2.8 Particle orientation distribution for the flow mark region of TPO #1.

For the core flow front region, the micrograph reveals that the particles are elliptical, aligned parallel to the flow direction, and have an area fraction of 0.208 (Table 2.4). The particle size distribution (Figure 2.23) indicates that almost all of the particles are small ( $< 5 \, \mu m^2$ ) so there was no reason to do a small and large particle comparison like the flow mark and out-of-flow mark regions. The aspect ratio distribution (Figure 2.18) is narrow with a range of 1-5 and area weighted average at 1.91. Only the x and z dimensions were measured for the core flow front (Figure 2.19). The y dimension could not be determined because none of the micrographs taken show the cross sectional transverse xy plane.

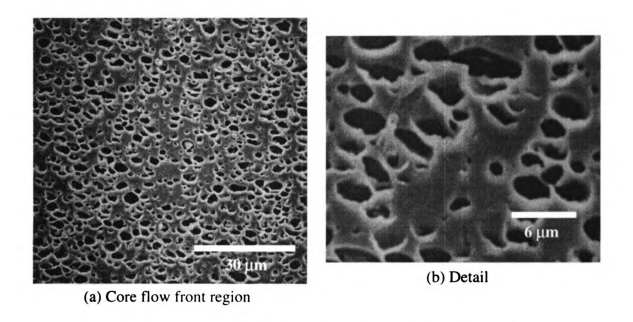


Figure 2.17 (a) Cross-sectional morphology at the core flow front for TPO #1.

(b) Detail of individual particles in the core flow front region.

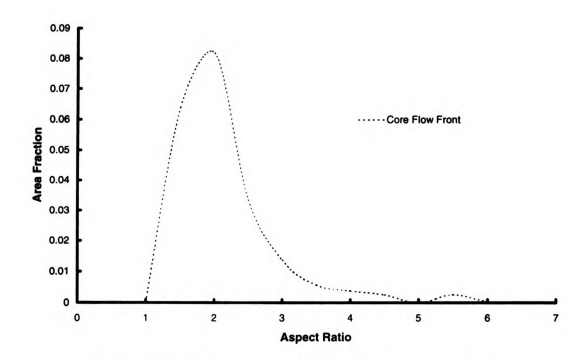


Figure 2.18 Aspect ratio distribution for the core flow front region of TPO #1.

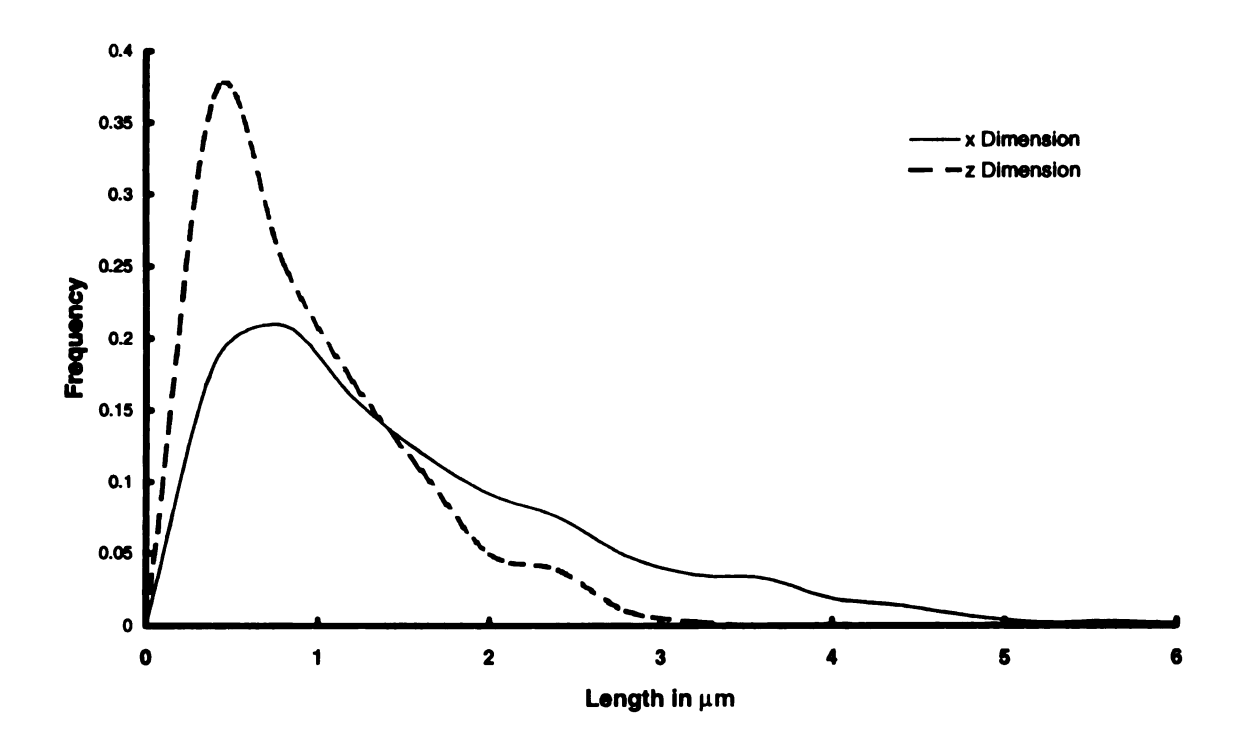


Figure 2.19 TPO #1 core flow front region particle lengths in the x and z dimensions (measured from Figure 2.17).

# 2.3.1 TPO#1 Particle Shapes

The shape of the particles in each region can be determined from the aspect ratios and the area weighted averaged lengths in the x, y, and z directions (Table 2.4). For the out-of-flow mark region, Figures 2.10(a) and 2.13(a) indicate that the particles are strand-like cylindrical cylinders with their lengths oriented in the x direction. The particles at the surface are highly stretched, with an area weighted aspect ratio of 15.2 between the x and y dimensions. The broad particle size and area weighted aspect distributions (Figures 2.33-2.25) indicate the presence of both small and large highly stretched particles. Figure 2.70 shows a representative particle and its' orientation.

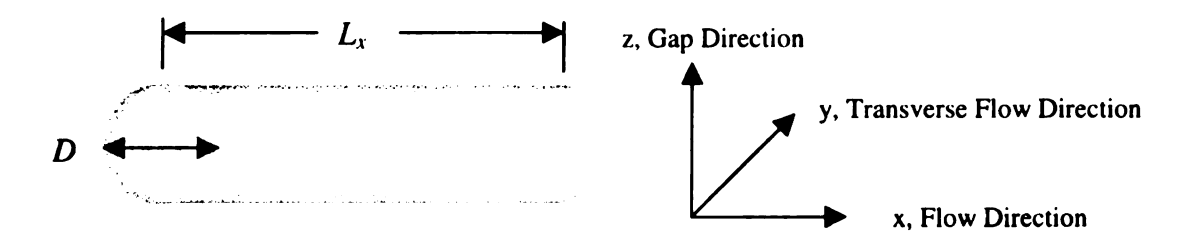


Figure 2.20 Circular cylinder particle in the out-of-flow mark region.

The flow mark region particles shown in Figures 2.10(c) and 2.13(b) are elliptical cylinders whose length is oriented in the z direction. The area weighted aspect ratio is 2.04, its distribution (Figure 2.25) is very narrow, indicating that particles are elliptical shaped in the xy plane. In comparison to the area weighted x and y dimensions, the z dimension listed in Table 4 is small. Therefore, the particles resemble thin discs that are slightly stretched along their x axis. The particle size distributions (Figures 2.23 and 2.24) are broad, indicating a mixture of small and large particles. Figure 2.21 shows a typical particle and its orientation in the flow mark region.

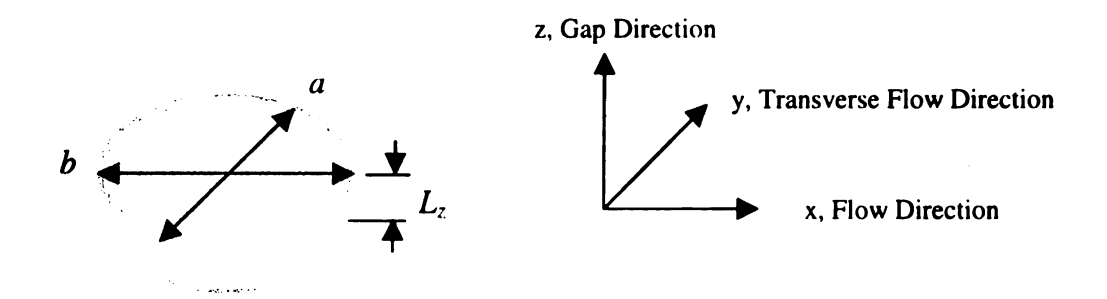


Figure 2.21 Elliptical cylinder particle in the flow mark region.

In the core flow front region, (Figure 2.4) the particles are ellipsoids. The area weighted x and z dimensions are listed in Table 2.4, but since there are no micrographs that show

the transverse yz plane, the y dimension could not be measured. The y dimension should be roughly equivalent to the z dimension. The particles are aligned parallel to the flow direction and the area weighted x dimension is almost double that of the z dimension, which corresponds to the area weighted aspect ratio of 1.91. The narrow particle size distributions (Figures 2.23 and 2.24) confirm the presence of a large number of small (< 5  $\mu m^2$ ) particles. Figure 2.22 shows a typical ellipsoid particle and it's orientation in the core flow front region.

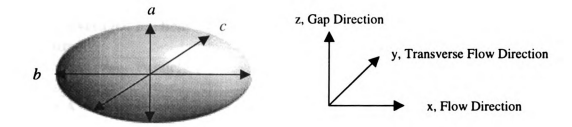


Figure 2.13 Ellipsoid particle in the core flow region.

Table 2.4 Measured values and calculated statistics for particles in TPO #1.

	Core Flow Front	Out-Of-Flow Mark Surface	Flow Mark Surface
Projected Area Fraction of Particles	0.208	0.168	0.115
Bulk Volume Fraction	0.31	0.31	0.31
Total Micrograph Area (μm²)	8244.6	8229.4	8280.1
Total Particle Area (µm²)	1714.5	1379.1	953.3
Total Number of Particles	1373	493	228
Number Averaged Particle Areas (µm²)	1.249	2.797	4.181
Weighted Average Particle Areas (µm²)	3.77	8.05	13.20
Number Averaged Aspect Ratio	1.84	11.53	2.14
Area Weighted Aspect Ratio	1.91	15.20	2.04
x-Dimension Area Weighted Averaged Length (µm)	2.77	11.03	5.71
y-Dimension Area Weighted Averaged Length (µm)	-	0.85	3.00
z-Dimension Area Weighted Averaged Length (µm)	1.53	-	1.31
Number Averaged Particle Volume (µm³)	0.35	1.34	3.23
Total Interfacial Area (μm²)	6495	5802	3606

The equations for volume, projected area in the xy, xz, and yz planes, and interfacial area for the different representative particle shapes are listed in Table 2.5.

Table 2.5 Geometric equations for various particle shapes.

Elliptical Cylinder (Length in x Direction)	Elliptical Cylinder (Length in z Direction)	Circular Cylinder	Ellipsoid
$\frac{\pi abL_x}{4}$	$\frac{\pi abL_z}{4}$	$\frac{\pi D^2 L_z}{4}$	$\frac{\pi abc}{6}$
$aL_x$	$\frac{\pi ab}{4}$	$DL_z$	$\frac{\pi bc}{4}$
$bL_{_{\mathrm{x}}}$	$bL_{z}$	$DL_z$	$\frac{\pi ab}{4}$
$\frac{\pi ab}{4}$	$aL_{z}$	$\frac{\pi D^2}{4}$	$\frac{\pi ac}{4}$
$2\pi L_x \sqrt{2a^2 + 2b^2} + \frac{\pi ab}{2}$	$2\pi L_z \sqrt{2a^2 + 2b^2} + \frac{\pi ab}{2}$	$\pi DL_z + \frac{\pi D^2}{2}$	$\pi a \overline{b}$
	(Length in x Direction) $ \frac{\pi abL_{s}}{4} $ $ aL_{s} $ $ bL_{s} $ $ \frac{\pi ab}{4} $	$(Length in x)$ $(Length in z)$ $Direction)$ $\frac{\pi abL_{\star}}{4}$ $aL_{\star}$ $\frac{\pi ab}{4}$ $bL_{\star}$ $bL_{\star}$ $\frac{\pi ab}{4}$ $aL_{\star}$	(Length in x Direction) $ \frac{\pi abL}{4} \qquad \frac{\pi abL}{4} \qquad \frac{\pi D^2 L}{4} $ $ aL, \qquad \frac{\pi ab}{4} \qquad DL, $ $ bL, \qquad bL, \qquad DL, $ $ \frac{\pi ab}{4} \qquad aL, \qquad \frac{\pi D^2 L}{4} $

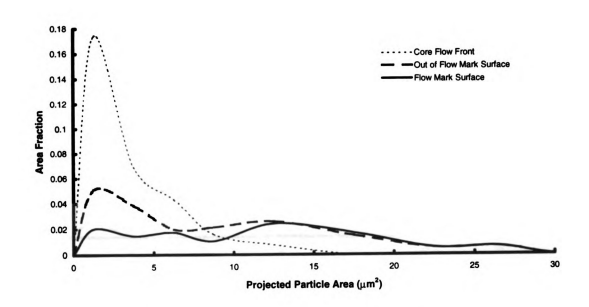


Figure 2.23 Particle size area distribution for TPO #1.

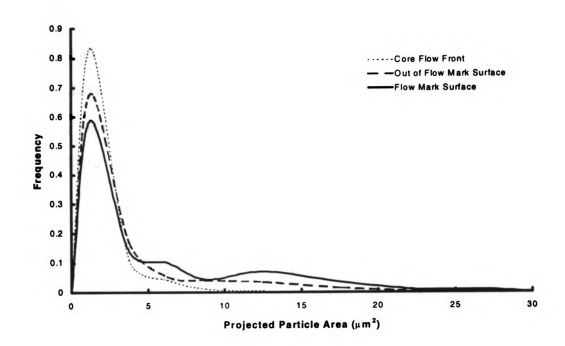


Figure 2.24 Particle size distribution for TPO #1.

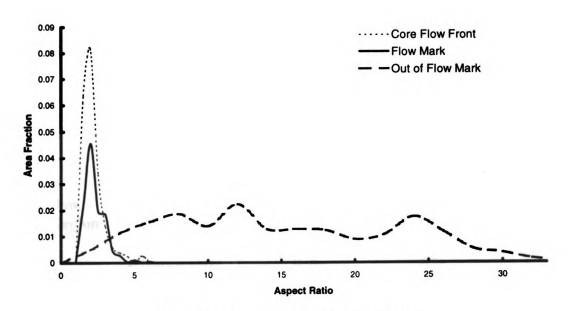


Figure 2.25 Aspect ratio distributions for TPO #1.

Table 2.6 shows the standard deviations for the number averaged aspect ratios and number averaged x, y, and z dimension lengths for TPO #1. For the out-of-flow mark region, the aspect ratio distribution (Figure 2.11) and x-dimension length distribution (Figure 2.12) are non-gaussian. Because of this, the standard deviation cannot be accurately calculated for them. Therefore, the most probable range where the particles lie has been listed.

**Table 2.6** Variability of x, y, and z dimension lengths for TPO #1.

		Number Averaged Value	Standard Deviation	Most Probable Range
	Aspect Ratio	11.53		5-27
0.007	x-Dimension	5.59		1-7
Out-Of-Flow Mark Region	Length (μm) y-Dimension	0.61	±0.32	
	Length (µm)			
	Length (µm)			
	Aspect Ratio	2.14	±0.84	
Flow Mark	x-Dimension Length (µm)	2.9	±2.1	
Region	y-Dimension Length (µm)	1.48	±0.46	
	z-Dimension Length (µm)	0.77	±0.48	
	Aspect Ratio	1.84	±0.71	
Core Flow	x-Dimension Length (µm)	1.37	±1.1	
Front Region	y-Dimension Length (μm)	-	-	
	z-Dimension Length (µm)	0.76	±0.58	

### 2.3.2 Flow Mark vs. Out-of-flow Mark Comparison

The particle volume is conserved between the flow mark and out-of-flow mark regions and there is negligible particle migration difference between the two. For the two regions, Table 2.7 shows the number averaged areas and the total number of particles.

**Table 2.7** Number average for the out-of-flow mark and flow mark regions.

	Out-Of-Flow Mark Surface	Flow Mark Surface
<b>Total Number</b> of Particles	493	228
Number Averaged Particle Area (µm²)	2.8	4.2
y-Dimension Number Averaged Length (µm)	0.61	1.48
z-Dimension Number Averaged Length (µm)	-	0.77

To obtain the total particle volume  $V_T$  in the flow mark region, the xy plane projected area is substituted into the volume equation for an elliptical cylinder whose length is oriented in the z dimension (Table 2.5) and is then multiplied by  $N_{FM}$  (the total number of particles).

$$V_T = A_{vv} L, N_{FM} (2-1)$$

Substituting in the flow mark surface values from Table 2.7 obtains:

$$V_T = 737 \mu \text{m}^3$$

Therefore, the average particle volume  $\left(\frac{V_T}{N_{FM}}\right)$  in the flow mark surface is 3.23  $\mu m^3$ .

The interfacial area was calculated using the equation for an elliptical cylinder whose length is oriented in the z direction (Table 2.5). The total interfacial area  $(A_{I_{Total}})$  was calculated by summing the interfacial area for every particle in the flow mark region. The value used for  $L_z$  was the number averaged length in the z direction.

$$A_{I_{TOTAL}} = \sum_{i=1}^{228} \left( 2\pi L_{z} \sqrt{2a^{2} + 2b^{2}} + \frac{\pi ab}{2} \right)_{i}$$
 (2-2)

$$A_{I_{TOTAL}} = 3606 \ \mu \text{m}^2$$

The ratio of total interfacial area to total particle volume is

$$\frac{A_{I_{TOTAL}}}{V_{T}} = 4.89 \ \mu \text{m}^{-1}$$

The shape with the minimum interfacial area is a sphere, therefore, as a comparison for retraction, the radius for a sphere of equal volume to a single particle in the flow mark region is calculated. The weighted average particle area and z dimension area weighted average length (Table 2.4) were used for  $A_{xy}$  and  $L_z$ .

$$\frac{4}{3}\pi R^{3} = A_{xy}L_{z}$$

$$R = 3.44 \ \mu\text{m}$$

$$\frac{3}{R} = 0.872 \ \mu\text{m}^{-1}$$

Thus the actual interfacial area in the flow mark region is 5.6 times greater than the fully retracted particle interfacial area.

To obtain the total particle volume  $V_T$  in the out-of-flow mark region, the xy plane projected area is substituted into the volume equation for a circular cylinder (Table 2.5) and is then multiplied by  $N_{OOFM}$  (the total number of particles).

$$V_T = \frac{\pi D A_{xy} N_{OOFM}}{4} \tag{2-4}$$

Substituting in the out-of-flow mark surface values from Table 2.6, using the y dimension number averaged length for D, yields:

$$V_{\tau} = 661 \, \mu \, \text{m}^3$$

Therefore, the average particle volume  $\left(\frac{V_T}{N_{OOFM}}\right)$  in the out-of-flow mark region is 1.34  $\mu m^3$ , which is 2.4 times smaller than the average particles volume for the flow mark region.

The interfacial area was calculated using the equation for a circular cylinder given in Table 2.5. The total interfacial area  $\left(A_{I_{TOTAL}}\right)$  for the out-of-flow mark region was calculated by summing the interfacial area for every particle in the out-of-flow mark region.

$$A_{I_{TOTAL}} = \sum_{i=1}^{493} \left( \pi D L_z + \frac{\pi D^2}{2} \right)_i$$

$$A_{I_{TOTAL}} = 5802 \ \mu \text{m}^2$$
(2-5)

The ratio of total interfacial area to total volume is

$$\frac{A_{I_{TOTAL}}}{V_{T}} = 8.78 \ \mu \text{m}^{-1}$$

To calculate the radius for a sphere with equal volume to a single particle in the out-offlow mark region, the weighted average particle area and y dimension area weighted average length (Table 2.4) were used for  $A_{xy}$  and D.

$$\frac{4}{3}\pi R^{3} = \frac{\pi A_{xx} D}{4}$$

$$R = 2.55 \ \mu\text{m}$$

$$\frac{3}{R} = 1.78 \ \mu\text{m}^{-1}$$

Thus the actual interfacial area in the out-of-flow mark region is 7.44 times greater than the fully retracted particle interfacial area.

The particles in the core flow front, flow to the melt front and become stretched by biaxial elongational flow. As they are being stretched, they flow along the short span of the melt front to the out-of-flow mark region and freeze in their stretched state at the mold wall.

Since the orientation distribution of the flow mark region shows that the particles are aligned parallel to the flow direction rather than randomly distributed, it can be concluded that the dominant mechanism is particle retraction as the particles flow along the long span from the stagnation point to the mold wall. The particles flow from the core flow front and become stretched by the biaxial elongational flow at the melt front in the same way as the out-of-flow mark particles. But due to the increased timescale as they flow along the long span from the stagnation point to the mold wall, the strands have enough time to retract into the observed disc shaped particles before they freeze at the wall

forming a flow mark region. Normally, if a free-floating particle retracts in a polymer matrix, it will form a sphere, but this does not happen for the EP rubber particles. They form discs instead. There are two reasons to explain this behavior. First, the mold wall constrains the particles and does not allow the spheres to form. Second, there is a large amount of shear at the wall, which hinders expansion in the z direction. The particles are constrained by these two factors and so they can only retract in the xy plane, which results in the formation of the observed discs. Even though they cannot form spheres, the particles still undergo a significant amount of retraction when compared to the fully stretched particles. Comparing the total interfacial area, there is 38% more area in the out-of-flow mark region than the flow mark region. Also, as the particles retract, they coalesce into larger particles that have 2.4 times the volume of the out-of-flow mark particles. Keeping the volume difference in mind, the ratio of the flow mark particle's calculated interfacial area to an equivalent sphere's  $\frac{3}{R}$  value is 5.60. That value is 1.3 times smaller than the out-of-flow mark region's ratio of 7.44.

To account for the reduction of the number of particles between regions and the increased average volume per particle in the flow mark region, coalescence must be taking place.

As the stretched particles retract, they could be coalescing with each other to form larger particles. The other option is that as two of the stretched strand-like particles retract to form the disc shaped particles of the flow mark region, one slides underneath the other and they stack like coins.

### 2.3.3 Core Flow Front vs. Mold Wall Comparison

The volume fraction of EP rubber (total particle volume) is the same in the core flow front region, flow mark region, and out-of-flow mark regions. For the core flow front region, Table 2.8 shows the number averaged areas and the x and z dimensions.

Table 2.8 Average particle dimensions for the core flow front region.

	Core Flow Front
Total Number of Particles	1373
Number Averaged	1.25
Particle Area (µm²) x-Dimension Number	1.37
Averaged Length (μm)	
y-Dimension Number Averaged Length (µm)	-
z-Dimension Number	0.76
Averaged Length (µm)	

To obtain the total particle volume  $V_T$  equation for the core flow front region, the xz plane projected area can be substituted into the volume equation for an ellipsoid (Table 2.5) and then be multiplied by  $N_C$  (the total number of particles).

$$V_T = \frac{2}{3} c A_{xc} N_C \tag{2-7}$$

An average value for c can then be obtained by substituting in 699  $\mu$ m<sup>3</sup> for the volume (the average volume between the flow mark and out-of-flow mark regions) and the core flow front values from Table 2.8.

$$c = 0.61 \, \mu \text{m}$$

Now that an average value for c has been obtained, the interfacial area for a single particle can be calculated. From Table 5, the interfacial area formula for an ellipsoid is:

$$A_{I} = \pi \iota i \overline{b} \tag{2-8}$$

where 
$$\overline{b} = \frac{\sqrt{2b^2 + 2c^2}}{2}$$

**Substituting** in the number averaged values for b and c yields:

$$\overline{b} = 0.69 \,\mu\text{m}$$

To obtain the total interfacial area, all of the areas must be summed.

$$A_{I_{TOTAI}} = \sum_{i=1}^{1373} (\pi a \overline{b})_{i}$$
 (2-9)

$$A_{I_{TOTAL}} = 4058 \ \mu \,\mathrm{m}^2$$

Dividing the total volume by the total number of particles yields an average particle volume of  $0.51 \ \mu m^3$ . If the assumption that volume is conserved between all of the regions is valid, then coalescence must be taking place.

Considering the case of the core flow front to the out-of-flow mark surface, the only time that coalescence can take place is when the particles approach the melt front and become stretched by elongational flow. On average, 2.8 of the core particles would have to coalesce to form one stretched particle.

In the flow mark region, the particles can coalesce twice. The first time would be as the particles approach the melt front and become stretched by elongational flow in the same

manner as the out-of-flow mark surface case. After being stretched, they can coalesce again as the particles retract into discs.

But volume may not be conserved between the core flow front and the wall regions because the average y dimension calculated for the ellipsoid particles in the core was 0.61  $\mu$ m. For an ellipsoid aligned parallel to the flow direction, it is assumed that the average y dimension should be at least equal to or greater than the z dimension. But since this is not the case, the core could contain much more volume than the wall regions. For example, if b and c were equal (prolate spheroid geometry), the total volume would be  $1748 \, \mu \text{m}^3$  and the interfacial area would be  $6858 \, \mu \text{m}^2$ . To explain the missing volume, there would have to be some sort of particle migration or break-up occurring. Particle break-up does not seem very likely because there would be an increased number of small particles seen in the flow front and out-of-flow front regions. Just the opposite is occurring in these regions, the particles are becoming larger and being reduced in number. Therefore, some combination of particle migration and coalescence is occurring, but the extent of which is unknown.

#### 2.4 Results of TPO #2 Image Analysis

The micrographs for the three regions of TPO #2 are shown in Figures 2.26, 2.29, and 2.33. As with TPO #1, the particle size distributions, Figures 2.39 and 2.40, indicate the pressence of small particles. Hereafter, the small particles will be catorgized by having projected areas  $< 7 \mu m^2$  and large particles will have projected areas  $> 7 \mu m^2$ .

The particles in the out-of-flow mark surface region (Figure 2.26(a)) are long, narrow, stretched parallel to the flow direction, and have an area fraction of 0.20 (Table 2.10). The large (> 7  $\mu$ m<sup>2</sup>) particles have a high area weighted average aspect ratio of 17.1 and take up 46% of the area fraction in the picture. The small particles (< 7  $\mu$ m<sup>2</sup>) also have a large area weighted average aspect ratio of 14.3. The aspect ratio distribution for all the particles (Figure 2.30) is very wide, ranging from 1-50, with an area weighted average at 15.60.

Table 2.9 shows the comparison to the small and large particles. It also contains the x, y, and z dimensions that were measured from the paricles in Figures 2.26 and 2.33. Figure 2.31 plots the x, y, and z dimension distributions for all of the out-of-flow mark particles.

Table 2.9 TPO #2 Out-of-flow mark region comparison of particles less than 7  $\mu$ m<sup>2</sup> vs. greater than 7  $\mu$ m<sup>2</sup>.

	Particles $< 7 \mu m^2$	Particles > $7 \mu m^2$	All Particles
Projected Area Fraction of Particles	0.108	0.092	0.200
Number of Particles	380	53	433
Number Averaged Aspect Ratio	11.87	17.06	12.51
Area Weighted Aspect Ratio	14.29	17.13	15.60
Number Averaged Areas (μm²)	2.33	14.26	3.79
Weighted Average Areas (µm²)	3.53	19.63	10.94
x-Dimension Number Averaged Length (µm)	5.71	17.99	7.22
y-Dimension Number Averaged Length (μm)	0.54	1.30	0.64
z-Dimension Number Averaged Length (µm)	0.56	0.56	0.56

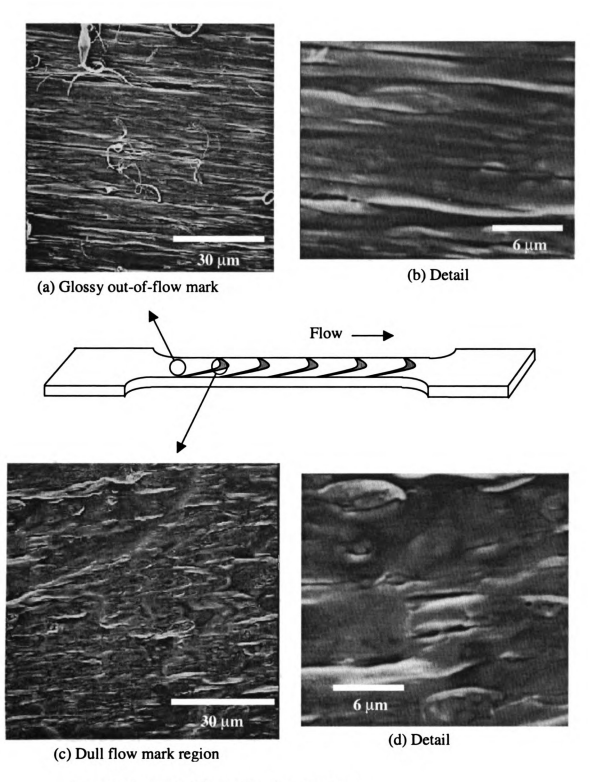


Figure 2.26 (a) Out-of-flow mark surface micrograph.

- (b) Detail of individual particles in the out-of-flow mark surface region.
- (c) Flow mark surface micrograph.
- (d) Detail of individual particles in the flow mark surface region.

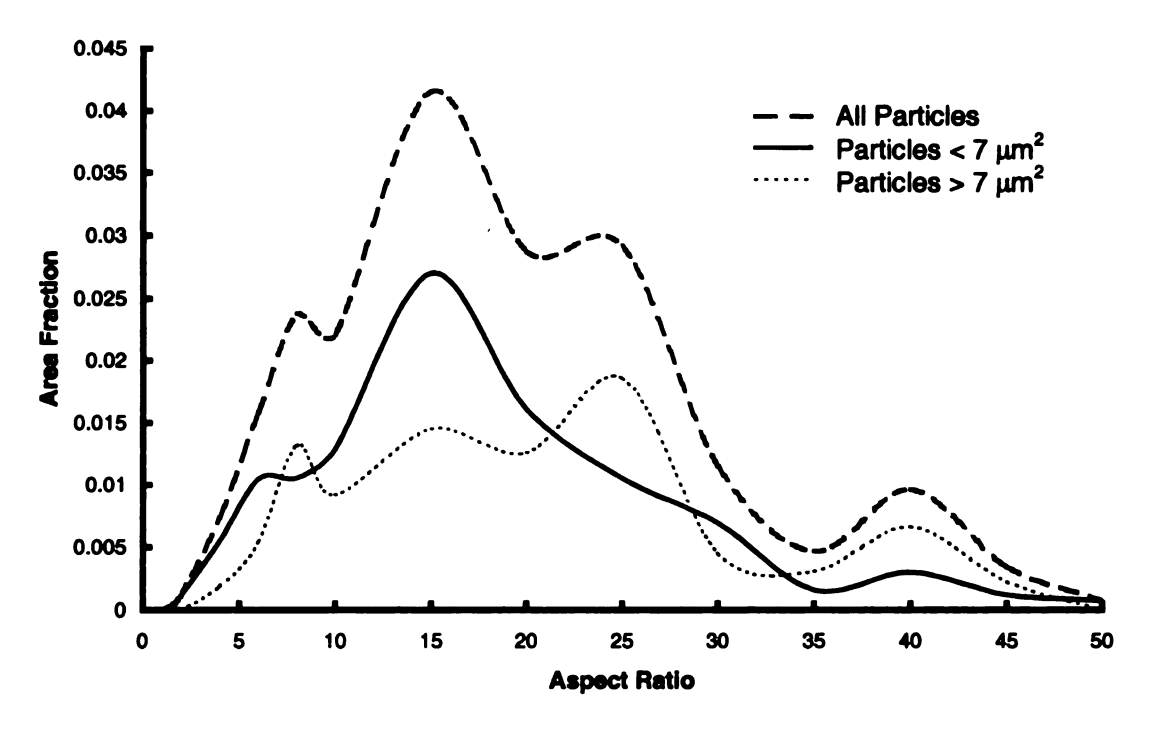


Figure 2.27 Aspect ratio distributions for the out-of-flow mark region of TPO #2.

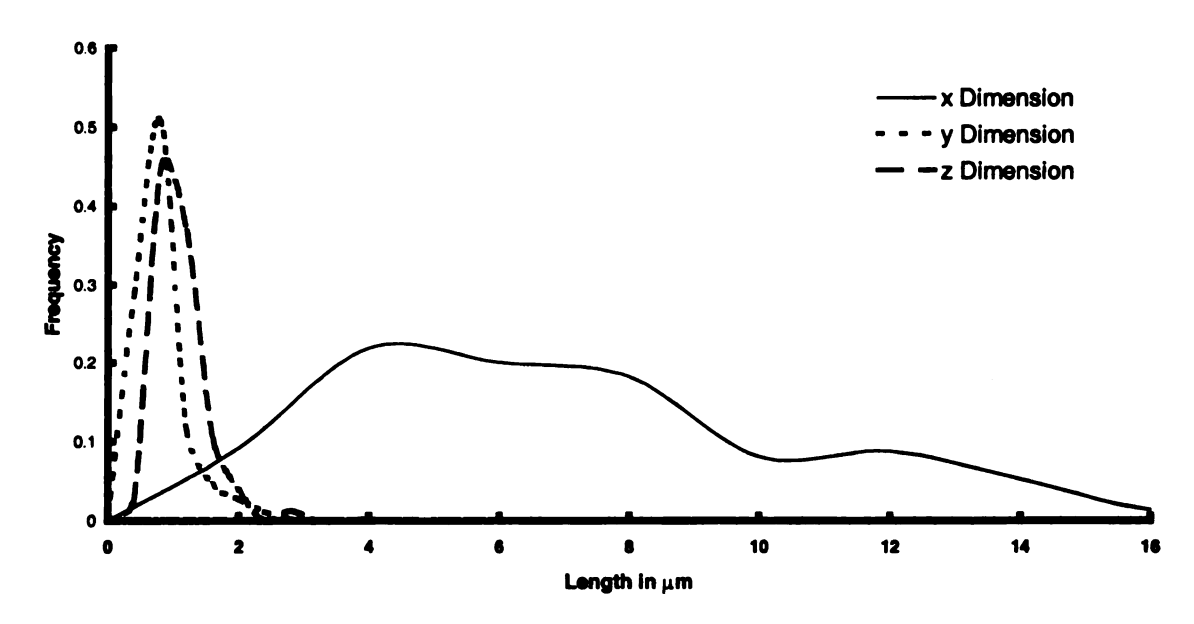


Figure 2.28 TPO #2 Out-of-flow mark region particle lengths in the x, y, and dimensions (measured from Figures 2.17(a) and 2.20(a)).

For both the flow mark and out-of-flow mark xz plane pictures (Figure 2.29), only the particles at the mold wall were examined to determine an average particle thickness in the z direction for each region. The particles in the xz plane cross-section underneath the surface were not counted. All of the particles in both regions are highly stretched and aligned parallel to the flow direction.

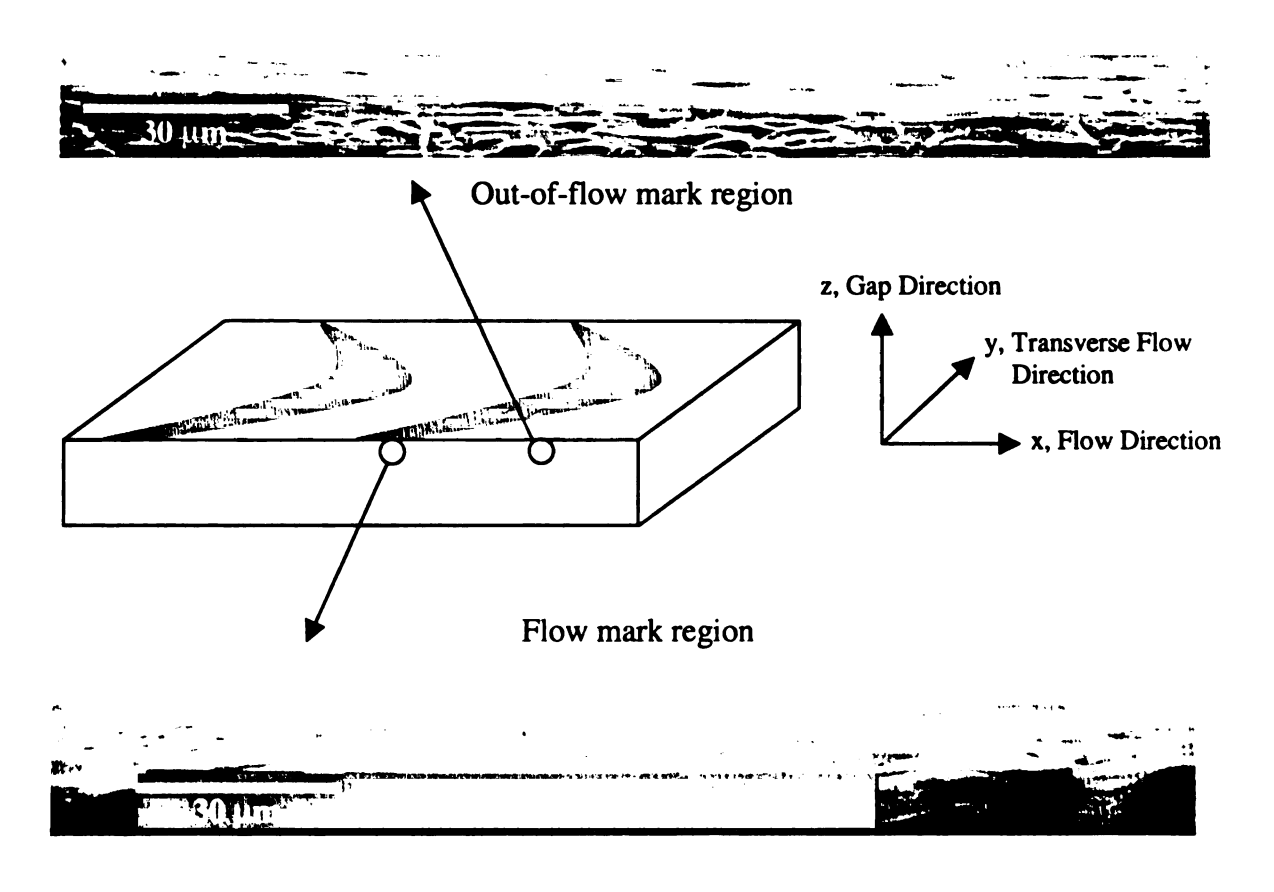


Figure 2.29 Cross-sectional morphology at the mold wall in the x, z plane for TPO #1.

The particles in the flow mark region are moderately stretched, aligned parallel to the flow direction, and have an area fraction of 0.1.26 (Table 2.10). The large (>  $7 \mu m^2$ ) particles have an area weighted aspect ratio of 9.54. The area weighted aspect ratio of the small (<  $7 \mu m^2$ ) particles slightly smaller at 9.16. The aspect ratio distribution (Figure 2.30) for all of the particles wide, ranging from 1-40, with an overall area weighted

aspect ratio of 9.27. Figure 2.32 shows the particle orientation distribution for all of the flow mark particles. Ther orientations were determined by measuring the angle difference between the paricle's major axis to the flow direction. The Hermann's planar orientation parameter  $(f_p)$  for TPO #2 is 0.949. It was calculated using:

$$f_p = 2\langle \cos^2 \theta \rangle - 1$$

The small and large particles for the flow mark region are compared in Table 2.10. It also contains the x and y dimensions that were measured from the particles in Figure 2.26(c). The z dimension number averaged length was determined by measuring the thickness of the particles at the mold wall (Figure 2.29(b)). This average thickness was taken as the z dimension of all of the particles, regardless of size. A plot of the x, y, and z dimension distributions for all of the flow mark particles is shown in Figure 2.31.

Table 2.10 TPO #2 Flow mark region comparison of particles less than 7  $\mu$ m<sup>2</sup> vs. greater than 7  $\mu$ m<sup>2</sup>.

	Particles < 7 μm <sup>2</sup>	Particles > 7 μm <sup>2</sup>	All Stretched Particles
Projected Area Fraction of Particles	0.090	0.036	0.126
Number of Particles	327	23	350
Number Averaged Aspect Ratio	8.07	9.40	8.16
Area Weighted Aspect Ratio	9.16	9.54	9.27
Number Averaged Areas (μm²)	2.28	12.99	2.99
Weighted Average Areas (μm²)	3.47	15.57	6.93
x-Dimension Number Averaged Length (μm)	4.88	13.31	5.43
y-Dimension Number Averaged Length (μm)	0.69	1.92	0.77
z-Dimension Number Averaged Length (μm)	0.87	0.87	0.87

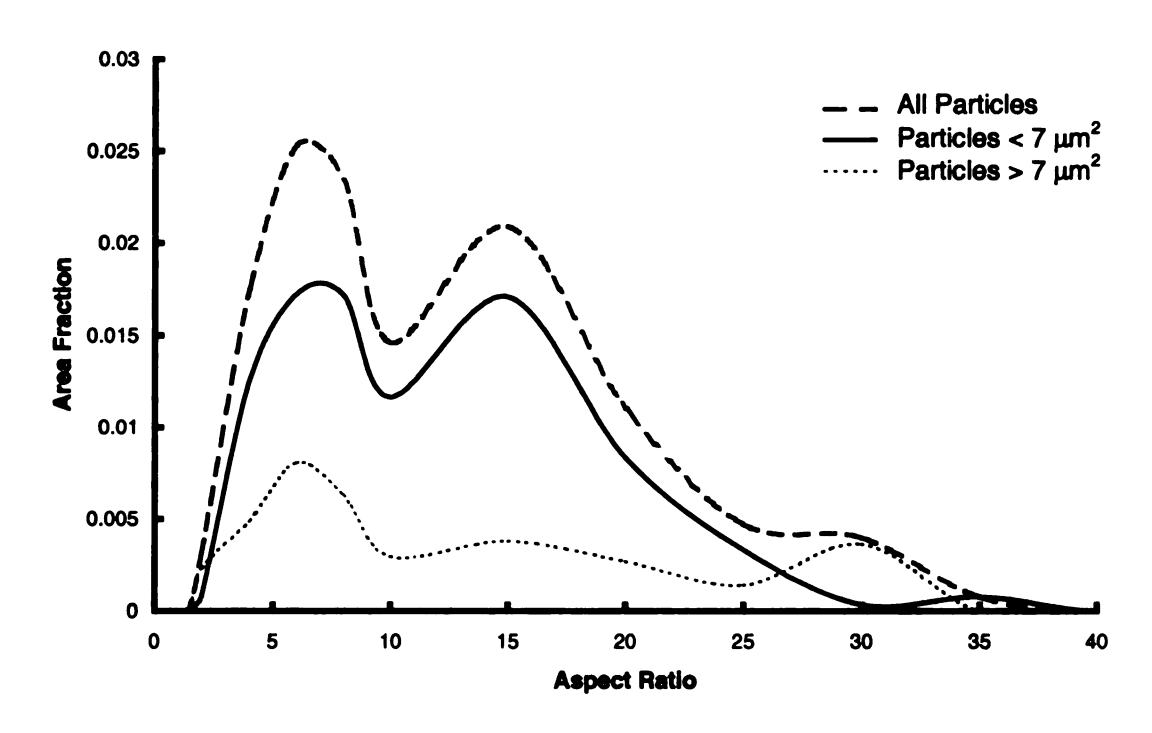


Figure 2.30 Aspect ratio distributions for the flow mark region of TPO #2.

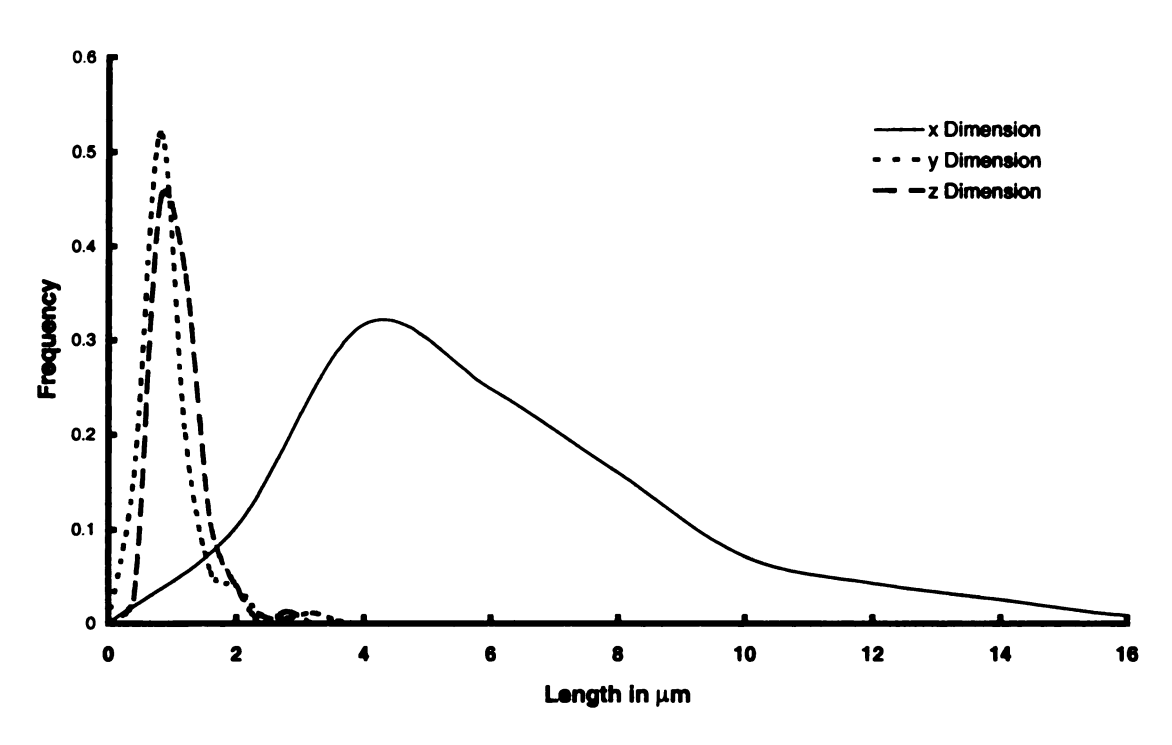


Figure 2.31 TPO #2 flow mark region particle lengths in the x, y, and z directions (measured from Figures 2.26(c) and 2.29(b)).

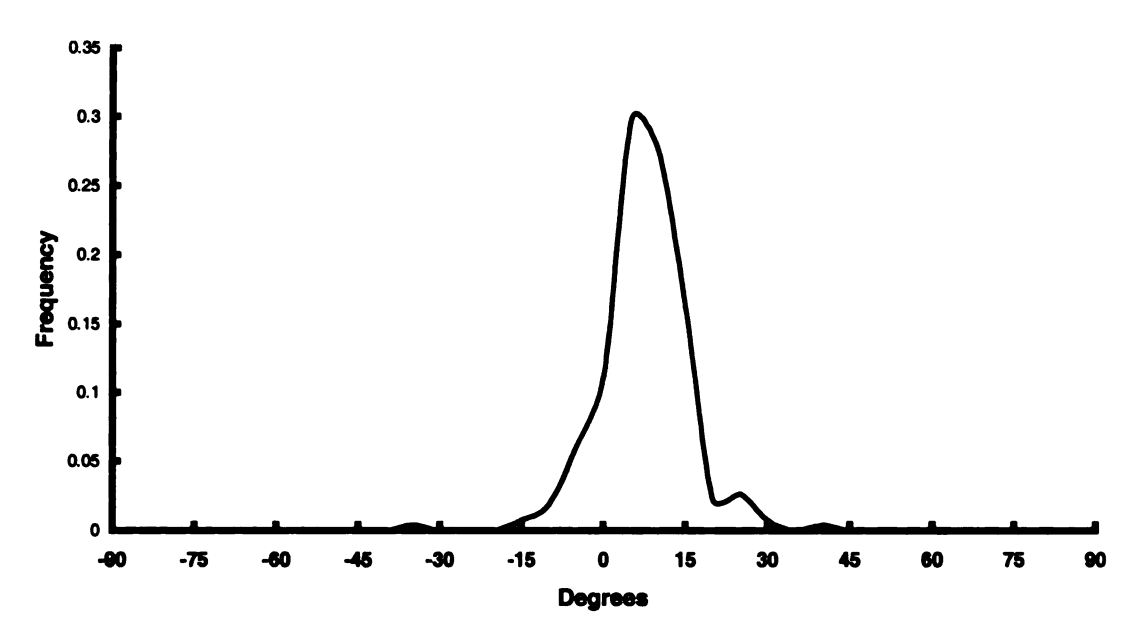


Figure 2.32 Flow mark particle orientation distribution for TPO #2.

For the core flow front region, the micrograph reveals that the particles are generally elliptical and have an area fraction of 0.217 (Table 2.9). Examination of the particle size distributions (Figures 2.39 and 2.40) indicates that almost all of the particles are small (< 7 µm²). The aspect ratio distribution (Figure 2.34) has a range of 1-9 and area weighted average at 4.22. Figure 2.35 plots the x and z plane dimensions for the core flow front. The y plane dimension could not be determined because none of the micrographs show the cross sectional transverse xy plane.

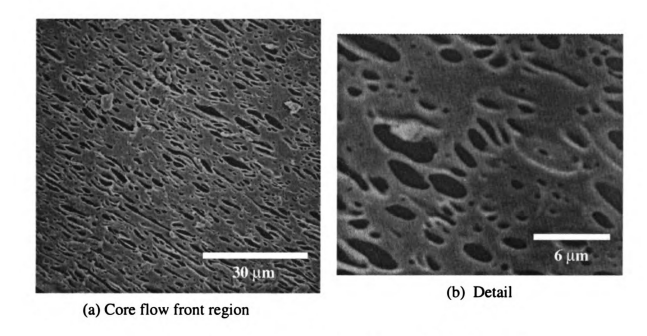


Figure 2.33 (a) Cross-sectional morphology at the core flow front for TPO #2.

(b) Detail of individual particles in the core flow front region.

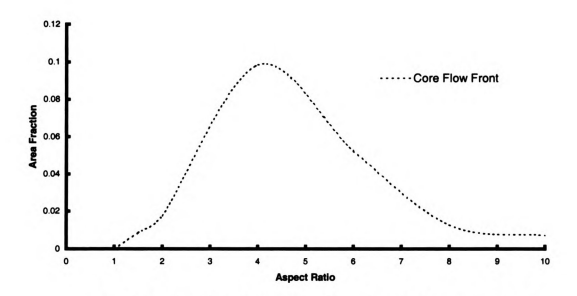


Figure 2.24 Aspect ratio distribution for the core flow front region of TPO #2.

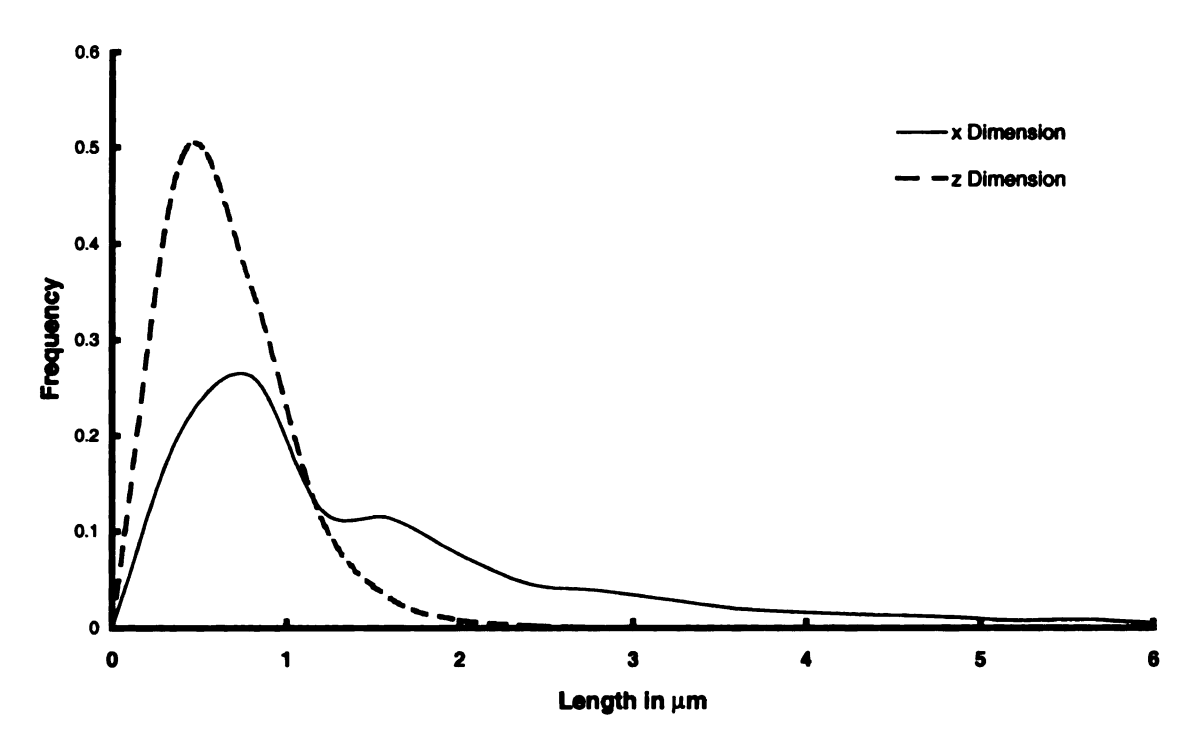


Figure 2.35 TPO #2 core flow front region particle lengths in the x and z directions (measured from Figure 2.33).

#### 2.4.1 TPO #2 Particle Shapes

A representative particle shape for each region can be determined from the aspect ratios and the area weighted averaged lengths in the x, y, and z directions (Table 2.11). The out-of-flow mark region particles shown in Figure 2.26(a) and 2.29(b) are elliptical cylinders with their length oriented in the x direction. As the area weighted aspect ratio of 15.60 suggests, the particles are highly stretched. Comparing the y dimension area weighted averaged length to the z dimension number averaged length (not enough particles were counted to obtain a true weighted averaged length), it is shown that the particle width in the y direction is twice its' thickness in the z direction. Figure 2.36 shows the representative particle shape and its' orientation.

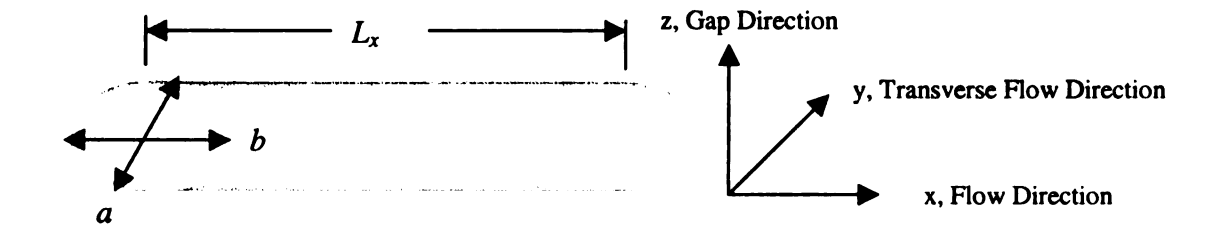


Figure 2.36 Elliptical cylinder particle in the out-of-flow mark region.

The flow mark region particles shown in Figure 2.23(c) and 2.26(d) are also elliptical cylinders with their length oriented in the x direction. These particles are moderately stretched when compared to the out-of-flow mark particles, with an area weighted aspect ratio of 9.27. Comparing the y dimension area weighted averaged length to the z dimension number averaged length (not enough particles were counted to obtain a true weighted averaged length), it is shown that the particle width in the y direction is roughly 1.4 times its' thickness in the z direction. Therefore, the particles are shorter, fatter, and thicker than the out-of-flow mark particles. Figure 2.37 shows the representative particle shape and its' orientation.

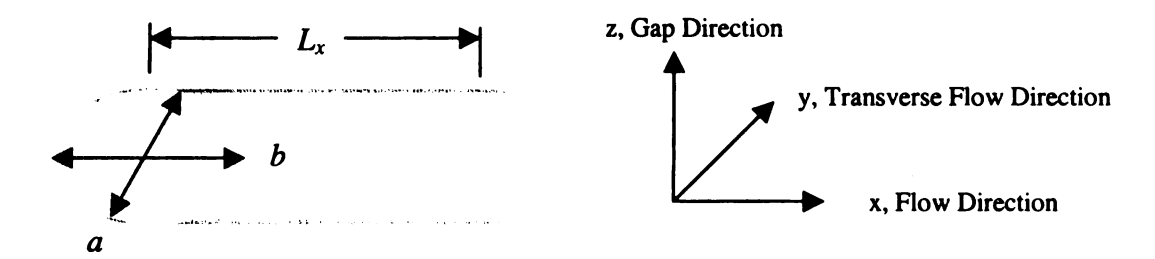


Figure 2.37 Elliptical cylinder particle in the flow mark region.

In the core flow front region, (Figure 2.33) the particles are ellipsoids. The area weighted x and z dimensions are listed in Table 2.11, but since there are no micrographs that show the transverse yz plane, the y dimension could not be measured. The y dimension should

be roughly equivalent to the z dimension. The particles are aligned parallel to the flow direction and the area weighted x dimension is over four times that of the z dimension, which corresponds to the area weighted aspect ratio of 4.22. The narrow particle size distributions (Figures 2.39 and 2.40) confirm the presence of a large number of small (< 7  $\mu$ m<sup>2</sup>) particles. Figure 2.38 shows a typical ellipsoid particle and its orientation in the core flow front region.

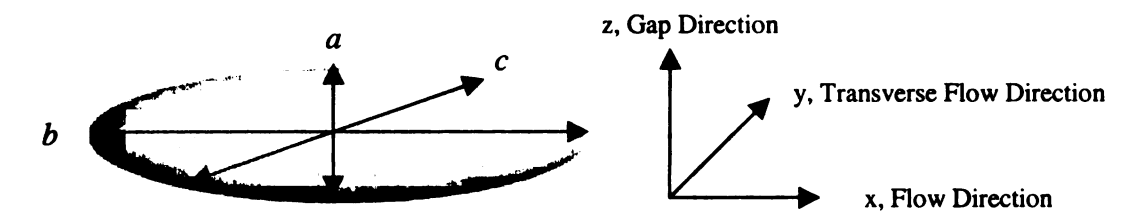


Figure 2.38 Ellipsoid particle in the core flow region.

Table 2.11 Measured values and calculated statistics for particles in TPO #2.

	Core Flow Front	Out-Of-Flow Mark Surface	Flow Mark Surface
Particle Area Fraction	0.217	0.200	0.126
<b>Bulk Volume Fraction</b>	0.34	0.34	0.34
Total Micrograph Area (μm²)	8244.7	8229.4	8280.1
Total Particle Area (μm²)	1790.5	1642.8	1045.8
Total Number of Particles	2068	433	350
Number Averaged Areas (μm²)	0.87	3.79	2.99
Area Weighted Averages (µm²)	3.69	10.94	6.93
Number Averaged Aspect Ratio	2.60	12.51	8.16
area Weighted Aspect Ratio	4.22	15.60	9.27
x-Dimension Area Weighted Averaged Length (µm)	2.57	13.92	8.85
y-Dimension Area Weighted Averaged Length (µm)	-	1.04	1.19
z-Dimension Number Averaged Length (µm)	0.50	0.56	0.87
z-Dimension Area Weighted Averaged Length (µm)	0.59	-	-
Number Averaged Particle Volume (µm³)	0.35	1.67	2.04
Total Interfacial Area (µm²)	6495	27962	22247

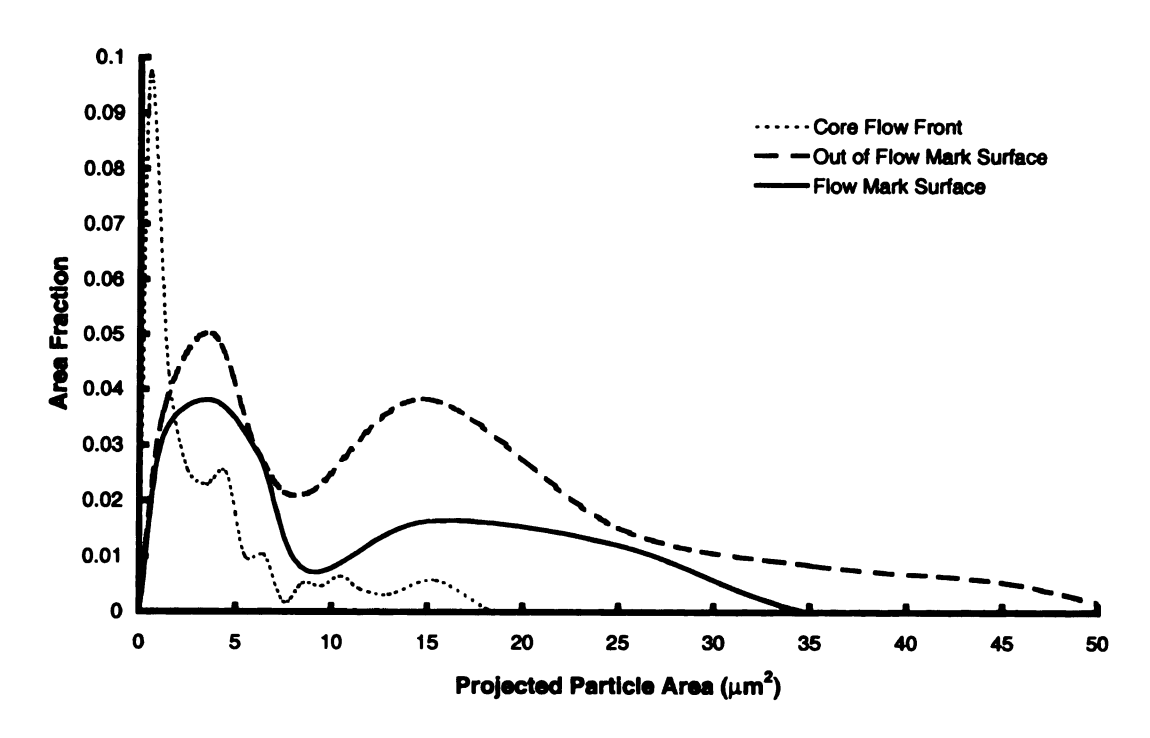


Figure 2.39 Particle size area distributions for TPO #2

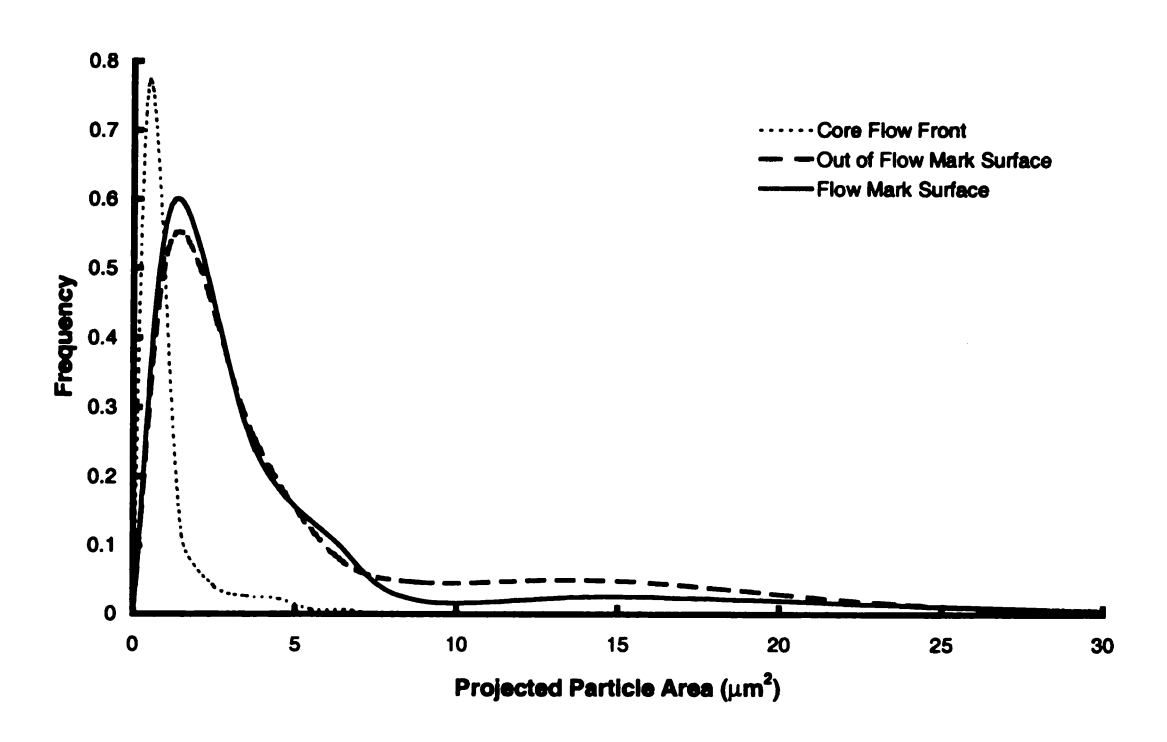


Figure 2.40 Particle size distributions for TPO #2.

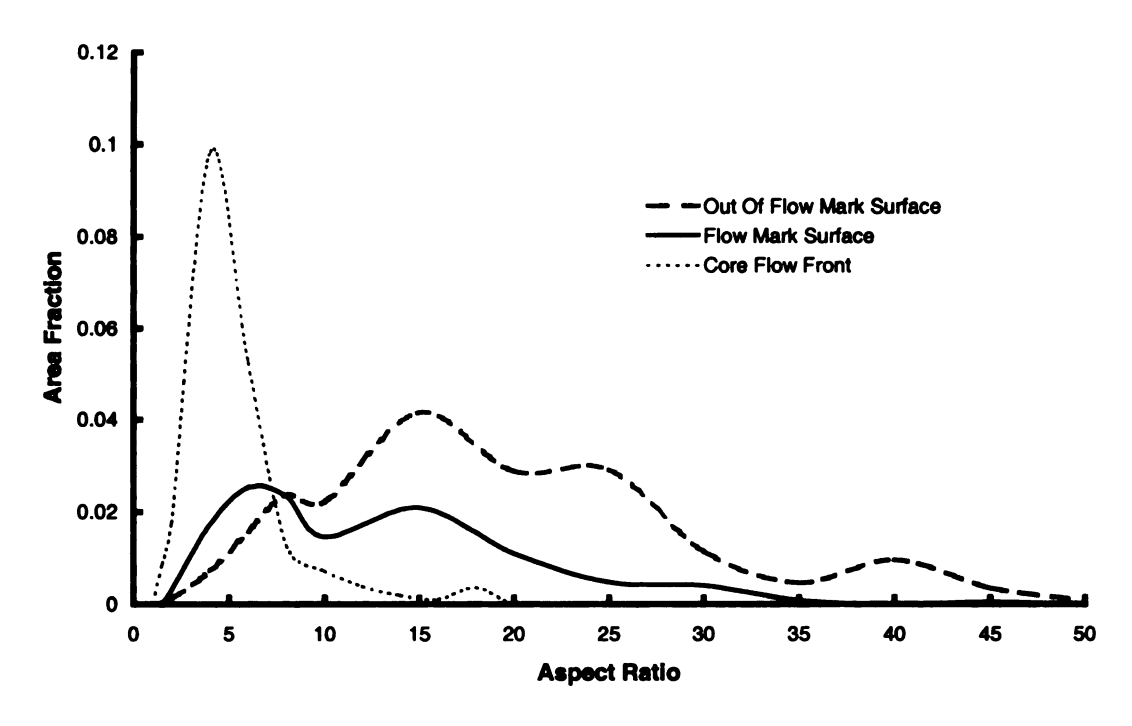


Figure 2.41 Aspect ratio distributions for TPO #2.

Table 2.12 shows the standard deviations for the number averaged aspect ratios and number averaged x, y, and z dimension lengths for TPO #2. The x-dimension length distributions for the out-of-flow mark region (Figure 2.28) and the core flow front (Figure 2.35) are non-gaussian. Because of this, the standard deviation cannot be accurately calculated for them. Therefore, the most probable range where the particles lie has been listed.

**Table 2.12** Variability of x, y, and z dimension lengths for TPO #2.

		Number Averaged Value	Standard Deviation	Most Probable Range
	Aspect Ratio	12.5	±8.5	
Out-Of-Flow	x-Dimension Length (µm)	7.22		2-10
Mark Region	y-Dimension Length (µm)	0.63	±0.41	
	z-Dimension Length (µm)	0.56	±0.14	
	Aspect Ratio	8.16	±5.39	
Flow Mark	x-Dimension Length (µm)	5.43	±3.7	
Region	y-Dimension Length (μm)	0.76	±0.5	
	z-Dimension Length (µm)	0.87	±0.4	
	Aspect Ratio	2.6	±1.67	
Core Flow	x-Dimension Length (μm)	1.45		0.5-2
Front Region	y-Dimension Length (μm)	-	-	
	z-Dimension Length (µm)	0.5	±0.3	

# 2.4.2 Flow Mark vs. Out-of-flow Mark Comparison

The particle volume is conserved between the flow mark and out-of-flow mark regions and there is negligible particle migration difference between the two. For the two regions, Table 2.13 shows the number averaged areas and the total number of particles.

Table 2.13 Number averaged statistics for the out-of-flow mark and flow mark regions.

	Out-Of-Flow Mark Surface	Flow Mark Surface
Total Number of Particles	433	350
Number Averaged Particle Area (µm²)	3.79	2.99
x-Dimension Number Averaged Length (µm)	7.22	5.43
y-Dimension Number Averaged Length (µm)	0.63	0.77
z-Dimension Number Averaged Length (µm)	0.56	0.87

To obtain the total particle volume  $V_T$  in the flow mark region, the xy plane projected area is substituted into the volume equation for an elliptical cylinder whose length is oriented in the x dimension (Table 2.5) and is then multiplied by  $N_{FM}$  (the total number of particles).

$$V_T = \frac{\pi A_{xy} b N_{FM}}{A} \tag{2-10}$$

Substituting in the flow mark surface values from Table 2.11 obtains:

$$V_T = 715 \mu \text{m}^3$$

Therefore, the average particle volume  $\left(\frac{V_T}{N_{FM}}\right)$  in the flow mark surface is 2.04  $\mu$ m<sup>3</sup>.

The interfacial area was calculated using the equation for an elliptical cylinder whose length is oriented in the x direction (Table 2.5). The total interfacial area  $\left(A_{I_{Total}}\right)$  was calculated by summing the interfacial area for every particle in the flow mark region. The value used for a was the number averaged length in the z direction.

$$A_{I_{TOTAL}} = \sum_{i=1}^{350} \left( 2\pi L_x \sqrt{2a^2 + 2b^2} + \frac{\pi ab}{2} \right)_i$$
 (2-11)

$$A_{I_{TOTAL}} = 22,247 \ \mu \text{m}^2$$

The ratio of total interfacial area to total volume is

$$\frac{A_{I_{TOTAL}}}{V_{T}} = 31.1 \,\mu\text{m}^{-1}$$

The shape with the minimum interfacial area is a sphere, therefore, as a comparison for retraction, the radius for a sphere of equal volume to a single particle in the flow mark region is calculated. The weighted average particle area and y dimension area weighed average length (Table 2.11) were used for  $A_{xy}$  and b.

$$\frac{4}{3}\pi R^3 = \frac{\pi A_{xy} b}{4} \tag{2-12}$$

$$R = 1.16 \ \mu \text{m}$$

$$\frac{3}{R} = 2.59 \ \mu \text{m}^{-1}$$

Thus the actual interfacial area in the flow mark region is 12.0 times greater than the fully retracted particle interfacial area.

To obtain the total particle volume  $V_T$  in the out-of-flow mark region, the xy plane projected area is substituted into the volume equation for an elliptical cylinder (Table 2.5) and is then multiplied by  $N_{OOFM}$  (the total number of particles).

$$V_T = \frac{\pi b A_{xy} N_{OOFM}}{4} \tag{2-13}$$

Substituting in the out-of-flow mark surface values from Table 2.11, using the y dimension number averaged length for b, yields:

$$V_T = 722 \ \mu \text{m}^3$$

Therefore, the average particle volume  $\left(\frac{V_T}{N_{OOFM}}\right)$  in the out-of-flow mark region is 1.67  $\mu m^3$ , which is 1.22 times smaller than the average particles volume for the flow mark region.

The interfacial area was calculated using the equation for an elliptical cylinder given in Table 2.5. The total interfacial area  $\left(A_{I_{TOTAL}}\right)$  for the out-of-flow mark region was calculated by summing the interfacial area for every particle in the out-of-flow mark region.

$$A_{I_{TOTAL}} = \sum_{i=1}^{433} \left( 2\pi L_x \sqrt{2a^2 + 2b^2} + \frac{\pi ab}{2} \right)_i$$
 (2-14)  
$$A_{I_{TOTAL}} = 27,962 \ \mu \text{m}^2$$

The ratio of total interfacial area to total volume is

$$\frac{A_{l_{TOTAL}}}{V_{T}} = 38.7 \ \mu \text{m}^{-1}$$

To calculate the radius for a sphere with equal volume to a single particle in the out-offlow mark region, the weighted average particle area and y dimension area weighted average length (Table 2.10) were used for  $A_{xy}$  and b.

$$\frac{4}{3}\pi R^3 = \frac{\pi A_{xy}b}{4}$$

$$R = 1.29 \ \mu\text{m}$$

$$\frac{3}{R} = 2.33 \ \mu\text{m}^{-1}$$

Thus the actual interfacial area in the out-of-flow mark region is 16.6 times greater than the fully retracted particle interfacial area.

The particles in the core flow front flow to the melt front and become stretched by elongational flow. As they are being stretched, they flow along the short span of the melt front to the out-of-flow mark region and freeze in their stretched state at the mold wall.

Since the orientation distribution of the flow mark region shows that the particles are highly aligned parallel to the flow direction rather than randomly distributed, it can be concluded that the dominant mechanism is partial particle retraction as the particles flow along the long span from the stagnation point to the mold wall. The particles flow from the core flow front and become stretched by the biaxial elongational flow at the melt front in the same way as the out-of-flow mark particles. But due to the increased timescale as they flow along the long span from the stagnation point to the mold wall, the

strands partially retract into the observed shorter, thicker particles before they freeze at the wall. Normally, if a free-floating particle retracts in a polymer matrix, it will form a sphere. Under the high shear conditions at the mold wall, the particles form discs, such as the particles in TPO #1. In this case though, the EP rubber particles in TPO #2 only have enough time to partially retract. Even though they cannot form spheres, the particles still undergo a significant amount of retraction when compared to the fully stretched particles. Comparing the total interfacial area, there is 21% more area in the out-of-flow mark region than the flow mark region. Also, as the particles retract, they coalesce into larger particles that have 1.22 times the volume of the out-of-flow mark particles. Keeping the volume difference in mind, the ratio of the flow mark particle's calculated interfacial area to an equivalent sphere's  $\frac{3}{R}$  value is 12.0. That value is 1.38 times smaller than the out-of-flow mark region's ratio of 16.6.

To account for the reduction of the number of particles between regions and the increased average volume per particle in the flow mark region, coalescence must be taking place.

As the stretched particles retract, they are coalescing with each other to form larger particles. On average, 1.2 stretched particles in the out-of-flow mark region coalesce to form a partially retracted flow mark particle.

# 2.4.3 Core Flow Front vs. Mold Wall Comparison

The volume fraction of EP rubber (total particle volume) is the same in the core flow front region, flow mark region, and out-of-flow mark regions. For the core flow front region, Table 2.12 shows the number averaged areas and the x and z dimensions.

Table 2.14 Average particle dimensions for the core flow front region.

	Core Flow Front
Total Number of Particles	2068
Number Averaged Particle Area (µm²)	0.87
x-Dimension Number Averaged Length (µm)	1.45
y-Dimension Number Averaged Length (µm)	-
z-Dimension Number Averaged Length (µm)	0.50

To obtain the total particle volume  $V_T$  equation for the core flow front region, the xz plane projected area can be substituted into the volume equation for an ellipsoid (Table 2.5) and then be multiplied by  $N_C$  (the total number of particles).

$$V_T = \frac{2}{3} c A_{xz} N_C \tag{2-16}$$

An average value for c can then be obtained by substituting in 719  $\mu$ m<sup>3</sup> for the volume (the average volume between the flow mark and out-of-flow mark regions) and the core flow front values from Table 2.12.

$$c = 0.60 \ \mu \text{m}$$

Now that an average value for c has been obtained, the interfacial area for a single particle can be calculated. From Table 2.5, the interfacial area formula for an ellipsoid is:

$$A_{l} = \pi a \overline{b} \tag{2-17}$$

where 
$$\overline{b} = \frac{\sqrt{2b^2 + 2c^2}}{2}$$

Substituting in the number averaged values for b and c yields:

$$\overline{b} = 0.55 \ \mu \text{m}$$

To obtain the total interfacial area, all of the areas must be summed.

$$A_{I_{TOTAL}} = \sum_{i=1}^{2068} (\pi a \overline{b})_{i}$$
 (2-18)

$$A_{I_{TOTAL}} = 6495 \ \mu \text{m}^2$$

Dividing the total volume by the total number of particles yields an average particle volume of  $0.35 \, \mu m^3$ . If the assumption that volume is conserved between all of the regions is valid, then coalescence must be taking place.

Considering the case of the core flow front to the out-of-flow mark surface, the only time that coalescence can take place is when the particles approach the melt front and become stretched by elongational flow. On average, 4.8 of the core particles would have to coalesce to form one stretched particle.

In the flow mark region, the particles can coalesce twice. The first time would be as the particles approach the melt front and become stretched by elongational flow in the same manner as the out-of-flow mark surface case. After being stretched, they can coalesce again as the stretched particles retract into the shorter, thicker particles.

The assumption that volume is conserved between the three regions is much more likely to be valid with TPO #2 than TPO #1 because of the geometry of the ellipsoid particles

(the average y dimension of 0.60 is greater than the average z dimension of 0.50).

Therefore, particle migration between the core and wall regions is not likely and the dominant mechanism between the core flow front and wall regions is coalescence.

#### **CHAPTER 3**

### CONCLUSIONS AND RECOMMENDATIONS

#### 3.1 Conclusions

The dominant mechanism of flow mark formation for TPO #1 is a combination of particle coalescence and retraction. As the ellipsoidal particles flow along the melt front, they coalesce and stretch into circular cylindrical particles, with their maximum area weighted aspect ratio reaching 11.5. As they flow from the stagnation point to the long span of the melt front to the wall, they have enough time to retract back into disc shaped particles aligned parallel to the flow direction, with area weighted aspect ratios of 2.14. As the particles retract, they can coalesce again or the discs can slide underneath each other to form stacks. A gauge for the amount of retraction that occurs in the system is the reduction of the total interfacial area of the particles in the flow mark compared to the out of flow mark region. For TPO #1, the reduction is 25% between the two regions.

Comparing the core flow front region to the wall regions, particle migration might be occurring, but this is unconfirmed because no SEM micrographs show the yz plane of the core flow front region and therefore, a true estimate of the total volume of the core flow front particles cannot be determined.

The dominant mechanism of flow mark formation for TPO #2 is also a combination of particle coalescence and retraction. As the ellipsoidal particles flow along the melt front, they coalesce and stretch into elliptical cylindrical particles, with their maximum area weighted aspect ratio reaching 15.6. As they flow from the stagnation point to the flow

mark region, they start to retract and form shorter, wider, and thicker elliptical cylindrical particles oriented parallel to the flow direction with an area weighted aspect ratio of 9.27. The particles freeze in this partially retracted state once they reach the mold wall. The reduction of the interfacial area between the two regions is 28%.

The key to reducing the amount of flow marks in the injection molding process may be in the rheology between the matrix and the EP rubber particles. In TPO #1 there is a difference in molecular weight of 110,000 between the two components. Naturally, one would also expect a large viscosity difference as well. Because of this viscosity difference, the relaxation time for the EP rubber particles is very small and the particles retract very quickly. This would explain why there is such a gross difference in the morphology between the out of flow mark and flow mark regions. For TPO #2, the molecular weight difference between the PP and EP rubber is 55,000, and therefore the viscosities between the two are more comparable. Because of this, the EP rubber particles are stretched further and the relaxation time is longer because the similar viscosities hinder the particle retraction process. For this reason, the flow mark particles in TPO #2 are still in a partially stretched state as they freeze at the mold wall. If the rheology of the matrix and EP rubber particles could be tailored to match each other more closely, the relaxation time could be large enough that if the particles flow along the long span of the melt front, they can still reach the mold wall in a highly stretched state and form an out of flow mark region instead of creating flow marks.

Table 3.1 shows the effects on flow line formation by changing the processing conditions, mold geometry, and polymer rheology of the injection molding system.

**Table 3.1** Effects of changing the molding conditions on flow line formation.

Condition Changed	Effect
Heat mold	+
Increase injection rate	_
Decrease injection rate	+
Increase part thickness	+
Decrease part thickness	_
Simplify mold geometry	0
Complicate mold geometry	0
Decrease the viscosity ratio between matrix/filler	_
Increase the viscosity ratio between matrix/filler	+
	Heat mold  Increase injection rate  Decrease injection rate  Increase part thickness  Decrease part thickness  Simplify mold geometry  Complicate mold geometry  Decrease the viscosity ratio between matrix/filler

- + reduces the formation of flow lines
- increases the formation of flow lines
- 0 no effect

## 3.2 Recommendations for Further Work

The goal of this research was to determine the dominant mechanism for flow mark formation during the injection molding process and provide insight on how to reduce the occurrence of their formation. Now that an explanation for the morphology changes between the regions has been determined, future work can be done in two areas:

• Additional micrographs in the yz plane could be taken and examined to determine if there is significant particle migration from the wall to the core regions.

- A new polymer blend of PP and EP rubber could be made that has its' rheology tailored to lengthen the EP rubber particle relaxation time. This blend could be molded and tested to see if there is a reduction in the occurrence of flow mark formation.
- Using Table 3.1 as a guide, quantitative studies could be performed for each
  variation of the molding conditions to see its effect on the occurrence of flow
  lines for both TPO's.

**APPENDIX** 

### **APPENDIX**

#### **IMAGE ANALYSIS**

### 1. Determination of Aspect Ratio

The SEM micrographs were scanned into TIF image files and analyzed using Sigma Scan 3.0 from Jandel Scientific. The border of a particle was outlined using the software and then the major and minor axis lengths were calculated. The major axis is defined by searching all of the border pixels of the particle and choosing the two pixels that are the farthest apart. Once a major axis is defined, the minor axis is calculated. The minor axis is drawn between the two pixels defining the longest line perpendicular to the major axis. The aspect ratio for the particle is then calculated by

$$\ell_i = \left(\frac{\text{major axis length}}{\text{minor axis length}}\right)_i$$

The number averaged aspect ratio is then determined by

$$\ell_{NA} = \sum_{i=1}^{n} \frac{\ell_{i}}{\ell_{TOTAL}}$$

The area weighted aspect ratio is determined by dividing the sum of the aspect ratio multiplied by the particle area by the sum of the particle area

$$\ell_{AWA} = \frac{\sum_{i=1}^{n} (A_i \ell_i)}{\sum_{i=1}^{n} A_i}$$

## 2. Determination of x, y, and z Dimensions

The x, y, and z dimensions of the particles were determined by measuring the major and minor axes of the particles. The major and minor axes were defined as the x, y, or z dimension depending on what plane the micrograph showed. For example, for a micrograph showing the xz plane of the core flow front, the major axis would be the x dimension and the minor axis would be the z dimension. The number averaged x, y, and z dimension lengths are calculated with the following equations

$$x_{NA} = \sum_{i=1}^{n} \frac{x_i}{x_{TOTAL}}$$

$$y_{NA} = \sum_{i=1}^{n} \frac{y_i}{y_{TOTAL}}$$

$$z_{NA} = \sum_{i=1}^{n} \frac{z_i}{z_{TOTAL}}$$

The area weighted x, y, and z dimensions are determined by dividing the sum of the dimension multiplied by the particle area by the sum of the particle area

$$x_{AWA} = \frac{\sum_{i=1}^{n} (A_i x_i)}{\sum_{i=1}^{n} A_i}$$

$$y_{AWA} = \frac{\sum_{i=1}^{n} (A_i y_i)}{\sum_{i=1}^{n} A_i}$$

$$z_{AWA} = \frac{\sum_{i=1}^{n} (A_i z_i)}{\sum_{i=1}^{n} A_i}$$

**BIBLIOGRAPHY** 

## **Bibliography**

Chan, C.-M. and J. Feng, J. Rheol., 41 (2), 319 (1997).

Chang, M.C.O., SPE Tech Papers, 40, p.36 (1994).

Choi, S.J., Schowalter, W.R., *Physics of Fluids*, **18** (4), 420-427, (1975).

Hamada, H. and H. Tsunasawa, J. Appl. Polym. Sci., 60 (3), 353-362 (1996).

Han, C.Y., M.D. Wolkowicz, D. Dong, and S.S. Dagli, SPE Tech Papers, 42, (1996).

Hoffman, R.L., J. Rheol., 29 (5), 579-604 (1985).

Hobbs, S.Y., Polym. Eng. Sci., 36 (11), 1489-94 (1996).

Koh, C.J., Hookham, P., and L.G. Leal, J. Fluid Mech., 266, 1-32, (1994).

Minale, M., Mewis, J., and P. Molenaers, AIChE J., 44 (4), 943-950, (1998).

Newman, S. and Q. Trementozzi, J. Appl. Polym. Sci., 9, 3071-3089 (1965).

Riemann, R.-E., Cantow, H.-J., and C. Friedrich, *Macromolecules*, **30**, 5476-5484, (1997).

Yokoi, H., S. Nagami, A. Kawsak, Y. Murata, SPE ANTECH, 1994, 368-372 (1994).

Yokoi, H., S. Nagami, A. Kawsak, Y. Murata, SPE ANTECH, 1994, 829-832 (1994).

